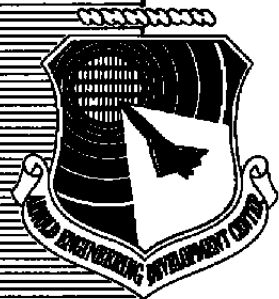


C#3



Laser Velocimeter Seed Particle Sizing by the Whisker Particle Collector and Laser Aerosol Spectrometer Methods

F. L. Crosswy
Calspan Corporation/AEDC Operations
and
M. K. Kingery, AEDC/DOTR
and
H. J. Schafer and H. J. Pfeifer
French-German Research Institute at Saint Louis, France

July 1989

Final Report for Period October 1, 1984 — September 30, 1987

**TECHNICAL REPORTS
FILE COPY**

**PROPERTY OF U.S. AIR FORCE
AEDC TECHNICAL LIBRARY**

Approved for public release, distribution is unlimited.

**ARNOLD ENGINEERING DEVELOPMENT CENTER
ARNOLD AIR FORCE BASE, TENNESSEE
AIR FORCE SYSTEMS COMMAND
UNITED STATES AIR FORCE**

NOTICES

When U. S. Government drawings, specifications, or other data are used for any purpose other than a definitely related Government procurement operation, the Government thereby incurs no responsibility nor any obligation whatsoever, and the fact that the Government may have formulated, furnished, or in any way supplied the said drawings, specifications, or other data, is not to be regarded by implication or otherwise, or in any manner licensing the holder or any other person or corporation, or conveying any rights or permission to manufacture, use, or sell any patented invention that may in any way be related thereto.

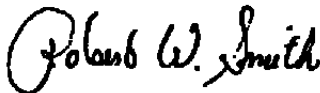
Qualified users may obtain copies of this report from the Defense Technical Information Center.

References to named commercial products in this report are not to be considered in any sense as an endorsement of the product by the United States Air Force or the Government.

This report has been reviewed by the Office of Public Affairs (PA) and is releasable to the National Technical Information Service (NTIS). At NTIS, it will be available to the general public, including foreign nations.

APPROVAL STATEMENT

This report has been reviewed and approved.



ROBERT W. SMITH
Directorate of Technology
Deputy for Operations

Approved for publication:

FOR THE COMMANDER



KEITH L. KUSHMAN
Technical Director
Directorate of Technology
Deputy for Operations

UNCLASSIFIED

SECURITY CLASSIFICATION OF THIS PAGE

REPORT DOCUMENTATION PAGE				Form Approved OMB No. 0704-0188	
1a. REPORT SECURITY CLASSIFICATION UNCLASSIFIED			1b. RESTRICTIVE MARKINGS		
2a. SECURITY CLASSIFICATION AUTHORITY			3. DISTRIBUTION / AVAILABILITY OF REPORT Approved for public release; distribution is unlimited.		
2b. DECLASSIFICATION / DOWNGRADING SCHEDULE					
4. PERFORMING ORGANIZATION REPORT NUMBER(S) AEDC-TR-89-3			5. MONITORING ORGANIZATION REPORT NUMBER(S)		
6a. NAME OF PERFORMING ORGANIZATION Arnold Engineering Development Center		6b. OFFICE SYMBOL (if applicable) DOT	7a. NAME OF MONITORING ORGANIZATION		
6c. ADDRESS (City, State, and ZIP Code) Air Force Systems Command Arnold Air Force Base, TN 37389-5000			7b. ADDRESS (City, State, and ZIP Code)		
8a. NAME OF FUNDING / SPONSORING ORGANIZATION Arnold Engineering Development Center		8b. OFFICE SYMBOL (if applicable) DO	9. PROCUREMENT INSTRUMENT IDENTIFICATION NUMBER		
8c. ADDRESS (City, State, and ZIP Code) Air Force Systems Command Arnold Air Force Base, TN 37389-5000			10. SOURCE OF FUNDING NUMBERS		
			PROGRAM ELEMENT NO N/A	PROJECT NO	TASK NO
					WORK UNIT ACCESSION NO
11. TITLE (Include Security Classification) Laser Velocimeter Seed Particle Sizing by the Whisker Particle Collector and Laser Aerosol Spectrometer Methods					
12. PERSONAL AUTHOR(S) Crossway, F. L., Calspan Corporation, AEDC Operations, Kingery, M. K., AEDC/DOTR, and (Cont.)					
13a. TYPE OF REPORT Final		13b. TIME COVERED FROM 10/1/84 TO 9/30/87		14. DATE OF REPORT (Year, Month, Day) July 1989	
				15. PAGE COUNT 85	
16. SUPPLEMENTARY NOTATION Available in Defense Technical Information Center (DTIC).					
17. COSATI CODES			18. SUBJECT TERMS (Continue on reverse if necessary and identify by block number)		
FIELD	GROUP	SUB-GROUP	laser velocimeter aerosol spectrometer		
20	07		particle sizing whisker particle collector		
20	08		laser aerosol spectrometer		
19. ABSTRACT (Continue on reverse if necessary and identify by block number) Two different aerosol particle sizing systems, the whisker particle collector (WPC) and the laser aerosol spectrometer (LAS), were evaluated for sizing aerosol particles in the size range 0.1 to 3.0 μ m. The evaluation tests were conducted using an aerosol of alumina (Al_2O_3) particles, an aerosol commonly used to provide light-scattering particles for laser velocimeter measurements in high-temperature flows. The measurement accuracy of the LAS was certified by comparison of its measurements to known particle sizes in test aerosols of precisely sized polystyrene latex spheres. The LAS and WPC measurements were then compared for samples taken from the alumina particle aerosols. Some difficulty was encountered in directly comparing these measurements because of the differences in the operating principles of the LAS (laser light scattering) and the WPC (particle capture/electron microscope analysis) and the consequent differences in the way the two systems account for prime particles and aggregates or agglomerates of prime particles. Other operational aspects of the two systems are also compared in this report including (Cont.)					
20. DISTRIBUTION / AVAILABILITY OF ABSTRACT <input type="checkbox"/> UNCLASSIFIED/UNLIMITED <input checked="" type="checkbox"/> SAME AS RPT <input type="checkbox"/> DTIC USERS			21. ABSTRACT SECURITY CLASSIFICATION UNCLASSIFIED		
22a. NAME OF RESPONSIBLE INDIVIDUAL C. L. Garner			22b. TELEPHONE (Include Area Code) (615) 454-7813		22c. OFFICE SYMBOL DOCS

DD Form 1473, JUN 86

Previous editions are obsolete.

SECURITY CLASSIFICATION OF THIS PAGE

UNCLASSIFIED

UNCLASSIFIED

12. PERSONAL AUTHORS (Concluded)

Schafer, H. J. and Pfeifer, H. J., French-German Research Institute at Saint Louis, France

19. ABSTRACT (Concluded)

on-line/off-line data presentation capabilities, field portability, and measurement limitations at the small particle end of the size range of interest.

UNCLASSIFIED

PREFACE

The work reported herein was performed under the AEDC/DEA Cooperative Technology Program as a joint effort by the Arnold Engineering Development Center (AEDC), Air Force Systems Command (AFSC) and the French-German Research Institute at Saint Louis, France (ISL). The AEDC/DOT Project Manager was M. K. Kingery. The AEDC results were obtained by Calspan Corporation, AEDC Operations, Operating contractor for the Aerospace Flight Dynamics Testing efforts at the AEDC, AFSC, Arnold Air Force Base, Tennessee. Experimental work, data analyses, and reporting work were conducted during the period October 1, 1984 through September 30, 1987, under AEDC Project Number DB15DV (Calspan Project Number D32V-CP). The manuscript was submitted for publication June 7, 1989.

CONTENTS

	<u>Page</u>
1.0 INTRODUCTION	5
1.1 Seed Particle Effects in Laser Velocimetry	5
1.2 Seed Aerosol Generation and Particle Size Measurements	5
1.3 ISL/AEDC Aerosol Particle Sizing Experiment	5
2.0 APPARATUS	7
2.1 Aerosol Generator	7
2.2 Electrostatic Aerosol Sampler	7
2.3 Laser Aerosol Spectrometer	7
2.4 Whisker Particle Capture System	11
2.5 Aerosol Sampling Experiment	12
3.0 TEST RESULTS	13
3.1 EAS Results	13
3.2 LAS Results	14
3.3 WPC Results	17
3.4 Comparison of WPC and LAS Results	19
4.0 OBSERVATIONS, SUMMARY OF RESULTS, AND CONCLUSIONS	20
REFERENCES	22

ILLUSTRATIONS

<u>Figure</u>	<u>Page</u>
1. Mechanically Agitated, Fluidized Bed Seeder	25
2. Electrostatic Aerosol Sampler (EAS)	26
3. Laser Aerosol Spectrometer (LAS) System	27
4. Laser Optics for the LAS	28
5. Quick-Look Histograms for the Five Certification Aerosols	29
6. High-Resolution Histograms for the Five Certification Aerosols	34
7. High-Resolution Composite Histograms for the Five Certification Aerosols	39
8. Differential Mobility Analyzer (DMA)	49
9. Nominal 0.18- μm Particles Produced by the DMA	50
10. Nominal 0.199- μm Particles Produced by the DMA	52
11. Electron Micrograph of a Whisker Particle Collector After Particle Sampling	54

Figure	Page
12. Schematic Diagram of the Setup for Aerosol Sampling	55
13. Electron Micrograph of Type C 1.0- μ m Alumina Particles Captured by the EAS (Magnification, 4,000x)	56
14. Electron Micrographs of Type A 0.3- μ m Alumina Particles Captured by the EAS	57
15. Particle Size Distributions for Various Alumina Powder Aerosols	59
16. Particle Size Distributions for Various Alumina Powder Aerosols with a Nominal Size Specification of 0.3- μ m	65
17. Electron Micrograph of the Type A, 0.3- μ m Alumina Particles Collected by the WPC	71
18. Electron Micrograph of the Type C, 1.0- μ m Alumina Particles Collected by the WPC	72
19. Particle Size Distribution on the First and Fourth Collector after Sampling the Type C 1.0- μ m Alumina Powder Aerosol	73
20. Particle Size Distribution on the First and Fourth Collector after Sampling the Type A 0.3- μ m Alumina Powder Aerosol	74
21. Log-Normal Distribution Function Fitted to the WPC Particle Size Distribution for the Type A 0.3- μ m Alumina Powder Aerosol	75
22. Cumulative Percentage Distribution Plotted on Log-Probability Paper for the Type C 1.0- μ m Alumina Powder Aerosol	76
23. Cumulative Percentage Distribution Plotted on Log-Probability Paper for the Type A 0.3- μ m Alumina Powder Aerosol	77
24. Log-Normal Functions Fitted to the LAS and WPC Histograms for the Type C 1.0- μ m Alumina Powder Aerosol	78
25. Log-Normal Functions Fitted to the LAS and WPC Histograms for the Type A 0.3- μ m Alumina Powder Aerosol	79

TABLE

1. Size Distribution Parameters Derived from Laser Aerosol Spectrometer (LAS) and Whisker Particle Collector (WPC) Methods	80
---	----

NOMENCLATURE	81
--------------------	----

1.0 INTRODUCTION

1.1 SEED PARTICLE EFFECTS IN LASER VELOCIMETRY

Because of the small light-scattering cross section of gas molecules, the laser Doppler velocimeter (LDV) cannot measure either individual molecular velocities or bulk gas velocity directly, but rather, it measures the velocity of small light-scattering (seed) particles entrained in the flowing gas. Gas velocity information is then inferred from the particle velocity measurements. Therefore, the performance of an LDV system is ultimately dictated by the dynamic response and light-scattering characteristics of the seed particles. Obviously, if the particles are too large, the gas velocity gradients cannot be closely tracked. On the other hand, if the particles are too small, too few photons will be scattered for detection by the LDV system. In addition to seed particle size per se, the seed particle size distribution is an important concern since the velocity sample broadening caused by a polydispersed seed aerosol in a velocity gradient can be confused with flow turbulence effects.

1.2 SEED AEROSOL GENERATION AND PARTICLE SIZE MEASUREMENTS

The preceding observations led to the conclusion that the seed aerosol should ideally be monodispersed and sized, if possible, to satisfy the conflicting dynamic response and detection requirements. The goal of finding the ideal seed aerosol has been elusive. Even the highly regarded (because of its monodispersity) polystyrene latex (PSL) spheres exhibit several undesirable characteristics such as the objectionable (in some cases) levels of suspension liquid that must be atomized and introduced into the test flow along with the particles, the low melting point ($\sim 105^{\circ}\text{C}$) of the PSL material, and the high cost (approximately \$100 for a 15-ml vial of suspension liquid with 3- to 10-percent PSL material by weight).

The development of seed aerosol generation techniques is crucially dependent upon the availability of a reliable and proven aerosol particle sizing system. The importance of this statement cannot be fully appreciated until one has observed the discrepancies that are commonly seen when the measured particle size distributions from two different aerosol particle sizing techniques are compared. Confidence in a particular particle sizing system is usually developed by favorable comparisons with an accepted sizing system or by certification of the unproven sizing system. Certification can be accomplished by comparisons of measured size distributions with test aerosols having known size and size distribution characteristics.

1.3 ISL/AEDC AEROSOL PARTICLE SIZING EXPERIMENT

With a mutual interest in developing expertise in aerosol particle size measuring techniques as a support technology for aerosol generator developments, personnel of the Arnold

Engineering Development Center (AEDC) and the French-German Research Institute at Saint Louis (ISL), France, recently conducted a joint laboratory experiment at the AEDC. An aerosol commonly used for LDV seeding purposes, especially in high-temperature flows, was sampled simultaneously by an ISL whisker particle capture (WPC) device and an AEDC electrostatic aerosol sampler (EAS). The aerosol was generated by fluidization of aluminum oxide (alumina) polishing powder. This particular powder product was selected since it is rather widely used for seeding purposes and because a nominal particle size is specified by the powder manufacturer.

Following the aerosol sampling operation, the WPC samples were returned to the ISL for analysis, and the electrostatically captured samples were retained at the AEDC for analysis. Comparisons of results were to be accomplished at a later date. Several weeks after the initial experiment, an aerosol particle sizer based upon laser light scattering was put into operation at the AEDC and used to analyze the same nominal aerosol as in the initial experiment. This aerosol particle sizer is referred to as a laser aerosol spectrometer (LAS). The day-to-day, week-to-week, and month-to-month repeatability of the alumina aerosol particle size distribution characteristic was found to be very good so that comparisons of WPC, EAS, and LAS results were considered valid even though the LAS aerosol samples were taken at a different time than the WPC and EAS samples.

Because of the geographic separation of the ISL and AEDC, the initial analyses proceeded independently. Initial data interpretations at the ISL, as well as at the AEDC, were complicated by the presence of flocs in the particle samples.* At the ISL, the aerosol generator was not available for further study, and it was eventually assumed that the flocs were caused by agglomeration of prime particles during the aerosol sampling process and that, therefore, these flocs should analytically be broken down into prime particles during the electron microscope analysis phase of the WPC process. The ISL data reduction procedures were conducted according to this premise, and this decision was communicated to the personnel of the AEDC. At the AEDC, however, initial results obtained with the LAS indicated that the flocs were intrinsic to the alumina powder aerosol. Since the aerosol generator was readily available for further study, it was decided that the origin and nature of the flocs should be determined conclusively and that methods to physically separate them into prime particles should be investigated. It was presumed that an AEDC particle size analysis of a deflocced

*For the purposes of this report, specific definitions for flocs, aggregates, and agglomerates have been adopted. An aggregate is defined as a clump of prime particles rather firmly bound together such as by thermal fusion. An agglomerate is defined as a clump of prime particles bound together by surface forces such as Van der Waals or liquid film bonds. A floc is defined as a clump of prime particles, and/or aggregates, and/or agglomerates held together by any one or a combination of the above-mentioned bonding mechanisms plus various other mechanisms such as mechanical interlinking of chainlike aggregates.

aerosol could then be directly compared with the ISL data. Moreover, the development of effective defloccing techniques was clearly of importance for the development of improved solid-particle aerosol generators.

The purpose of this report is to document the results of the joint ISL/AEDC aerosol particle sizing study. The WPC and LAS systems are described, and data from these two systems are presented and compared. Several schemes for defloccing solid-particle aerosols are described, and the associated LAS-derived particle size spectra are presented. The EAS device in conjunction with an electron microscope was primarily used for visual study of floc characteristics and pertinent photomicrographs are presented.

2.0 APPARATUS

2.1 AEROSOL GENERATOR

The apparatus used at the AEDC to produce solid-particle aerosols at low pressure (< 100 psi) is shown in Fig. 1. This device is referred to as a mechanically agitated, fluidized bed seeder. Solid particles in powder form are continuously stirred by a rotating hollow tube assembly. Carrier gas, usually air or nitrogen, flows through the tube assembly and jets into the powder through small holes to create the solid-particle aerosol.

2.2 ELECTROSTATIC AEROSOL SAMPLER

The model 3100 Electrostatic Aerosol Sampler (EAS) manufactured by TSI, Inc. (St. Paul, Minnesota, USA) was used to capture aerosol particles for subsequent electron microscope analysis. A functional diagram of this device is shown in Fig. 2. A vacuum pump in conjunction with a flowmeter and throttling valve draws the aerosol through the device at a constant flow rate. Inside the device, a corona discharge is established between a fine tungsten wire and a charging plate. As the aerosol passes through this charging section, the aerosol particles interact with the positive ions in the discharge and become positively charged. The charged aerosol then passes into the collecting section where a positive voltage is applied to the upper plate of a pair of precipitation plates. The resultant electrostatic field drives the positively charged aerosol particles to the lower plate. An electron microscope sample disk (graphite disk) is placed upon the lower plate to collect a sample of the precipitated particles. The sample disk is then removed and taken to the electron microscope for analysis.

2.3 LASER AEROSOL SPECTROMETER

A functional diagram of the LAS system is shown in Fig. 3. This system consists of an aerosol sampling unit and a separate electronic control unit. The LAS system is produced

by Particle Measuring Systems, Inc. (PMS) of Boulder, Colorado, USA. At the AEDC, the LAS was interfaced to a Digital Equipment Corporation (Maynard, Massachusetts, USA) Model 11/23 microcomputer system and a Tektronix, Inc. (Beaverton, Oregon, USA) Model 4631 hardcopy unit (Ref. 1). The essential features of the LAS aerosol sampling unit can be described by referring to Fig. 4. The illuminating light source is a 2-mw He-Ne laser with a beam diameter of about 1.2 mm at the region where it intersects the sample aerosol stream. The sample aerosol stream is surrounded by and aerodynamically focused by a stream of clean sheath air. The aerosol stream and sheath airstream are both drawn through the LAS by a built-in pump. The diameter of the aerosol stream is about 0.2 mm in the region where it intersects the laser beam.

The LAS operates on the principle that the level of light scattered by a particle within a laser optical cavity is a direct function of the particle size. In the LAS, the scattered light is collected by a parabolic mirror with a collection solid angle of about 2π sr. The collected light is reflected by the parabolic mirror and a 45-deg diagonal flat mirror to an aspheric lens that focuses the light onto a photodiode. The photodiode output is amplified by a digitally programmed amplifier section operating at gain settings commensurate with the size ranges selected. The output beam from the laser drives a reference photodiode, which in turn, furnishes a threshold signal for a pulse height analyzer. The particle size information is derived from the pulse height analyzer. The reference photodiode scheme serves as an automatic gain control to compensate for laser power changes.

The LAS system operates over the particle size range from 0.09 to 3.0 μm . This size range is covered by four, 15-bin instrument ranges of 0.09 to 0.195 μm (bin width, 0.007 μm), 0.15 to 0.3 μm (bin width, 0.01 μm), 0.24 to 0.84 μm (bin width, 0.04 μm), and 0.6 to 3.0 μm (bin width, 0.16 μm). The LAS is calibrated by the manufacturer with PSL spheres so that particle size measurements, even for irregularly shaped particles or particles with a complex index of refraction, are in terms of equivalent PSL spheres.

The DEC 11/23 was programmed to display the particle size data in three different formats. In one format, high-resolution histogram data from each of the four instrument ranges are displayed. In the second format, a 45-bin, high-resolution composite histogram derived from the four instrument ranges is displayed. In the third format, a low-resolution, "quick-look," 18-bin histogram covering the size range from 0.12 to 3.0 μm is displayed.

When the LAS system was first put into operation and for some time thereafter, there was some suspicion that unreasonably high counts were sometimes being observed in the first several bins of the smallest instrument range (0.090 to 0.195 μm). This same suspicion has recently been expressed by Yamada et al. (Ref. 2) about the first bin (0.090 to 0.097 μm) of this same instrument range. This suspicion of improper operation is the reason that

the quick-look histogram display was programmed to skip over the 0.090- to 0.118- μm range and to pick up at 0.12 μm . However, a very recent test (See Section 2.3.2.1) showed that, when properly adjusted, the LAS system in use at the AEDC did not produce unreasonably high counts in the smallest size bins. The high counts observed in these bins when sampling a supposedly monodispersed PSL aerosol is now attributed to impurity residues from the suspension liquid. Hodgkinson (Ref. 3) has previously pointed out that suspension liquid impurities can produce spurious small particle content in an otherwise monodispersed PSL aerosol.

2.3.1 LAS Certification

Certification of the LAS system was accomplished by measurements on test aerosols produced by atomization of PSL sphere suspensions. The sizes of the PSL spheres were specified by the manufacturer to be 0.176, 0.312, 0.497, 1.091, and 2.02 μm . The certification process using the PSL spheres was approached with some caution, however, since several investigators have noted discrepancies between their measurements of PSL particle size and those specified by the PSL manufacturer. For example, Heard et al. (Ref. 4) studied eight nominal sizes of PSL spheres over the size range from 0.109 to 1.099 μm and found discrepancies from 6 to -10 percent when their sizing results were compared to the PSL manufacturer's specifications. In a similar study, Yamada et al. (Ref. 2) sampled aerosols derived from nine different PSL suspensions with nominal PSL sphere sizes from 0.085 to 0.330 μm and noted size discrepancies from 6 to -18 percent.

It is important to note that one of the PSL suspensions used in the AEDC certification test was previously found by Porstendorfer (Ref. 5) to differ by -14 percent from the manufacturer's size specification. The PSL particles in question are specified to be 0.176 μm , whereas Porstendorfer's value is 0.151 μm . Porstendorfer's value for this particular PSL suspension is used by PMS, Inc., as part of their calibration procedure for the LAS so that when a 0.176- μm PSL aerosol is used, a properly calibrated LAS will read 0.151 μm . A PMS, Inc., Model PG-100 atomizer was used to generate the certification aerosols.

2.3.2 Certification Results

Quick-look histograms for the five certification aerosols are shown in Fig. 5. Local histogram peaks are observed to occur in the expected bin for each aerosol. However, these particle size distributions cannot strictly be described as monodispersed because of the width of the local distribution around the expected peaks and because of the significant number of counts in the lowest particle size bins. Moreover, the small particle counts are clearly dominant in the 1.091- and 2.02- μm histograms.

High-resolution, but limited range, histograms for the certification aerosols are shown in Fig. 6. Noting that Porstendorfer's value of $0.151\ \mu\text{m}$ applies to the nominal $0.176\text{-}\mu\text{m}$ aerosol, the histogram peak for this aerosol, as well as the peaks for the 0.312- and $1.091\text{-}\mu\text{m}$ aerosols, is found exactly in the expected bin, whereas the histogram peaks for the 0.497- and $2.02\text{-}\mu\text{m}$ aerosols are only off by one bin. The 0.312- , 0.497- , and $1.091\text{-}\mu\text{m}$ spectra are reasonable local approximations of monodisperse size distributions, whereas the 0.176- and $2.02\text{-}\mu\text{m}$ spectra are rather broad. A conclusive explanation for the widths of these distributions was not found during this study. However, a left skew of the distributions could conceivably be caused by a slight misalignment of the aerosol sample stream and laser beam in the LAS sampling head, even though a reasonable (but not exhaustive) effort to align the LAS was made before the measurements were attempted. The left skew characteristics observed here are very similar to those recorded by Yamada et al. (Ref. 2) while using an LAS instrument and PSL particles over the same size range as in this study. Skewness to the right of the histogram peaks, as in Figs. 6a and e, is, at this time, attributed to true particle size distribution effects since no LAS error mechanism can be identified that explain this.

The behavior of the small-particle counts in Figs. 5a through e was studied further by examining the high-resolution composite histograms for the five certification aerosols. As shown in Fig. 7, there is a very small contribution of spurious small particles to the size spectrum for the $0.176\text{-}\mu\text{m}$ PSL aerosol. However, the small-particle contributions become more and more prominent as PSL particle size increases and finally become dominant for the 1.091- and $2.02\text{-}\mu\text{m}$ aerosols. This effect is thought to have been caused by the fact that the PSL spheres are supplied, regardless of sphere size, at a fixed mass fraction with respect to the suspension liquid and, consequently, at a fixed mass fraction with respect to impurities in the suspension liquid. For these certification tests, all five PSL suspensions were diluted to roughly equal mass fractions, which meant that the number density of the small spheres was much greater than that of the larger spheres. It was found that a short-duration "puff" of aerosol into the plastic aerosol sample bag (See Fig. 3) was all that was needed to get a sufficient number of small PSL spheres for analysis by the LAS. This short puff generated a certain number density of spurious impurity particles that were also detected by the LAS. When aerosols containing the larger PSL spheres were sampled, a longer duration puff was required to produce a sufficient number density of PSL spheres in the sample bag. The volume of the bag did not vary with the duration of the sample puff since more or less of the bone-dry nitrogen was expelled. Therefore, the number density of impurity particles was greater for a long-duration puff than for a short-duration puff. This situation accounts for the large percentage of spurious small particles in the sample aerosols of the larger PSL spheres.

2.3.2.1 Certification by Differential Mobility Analyzer

Another highly regarded generator of monodispersed aerosols is the differential mobility analyzer (DMA). Published descriptions of this type of aerosol generator indicated that,

contrary to the experience with the PSL aerosols, there should be no spurious small-particle content in the output aerosol. It was considered important to conduct a test of the LAS using the DMA to determine whether or not it was capable of producing spurious bin counts in the lowest particle size bins.

A TSI, Inc., Model 3071 DMA was, therefore, obtained and put into operation to generate test aerosols for the LAS. A functional diagram for the DMA is shown in Fig. 8. A polydispersed aerosol is pumped through the DMA at a precisely controlled volumetric flow rate. As this aerosol flows through the bipolar charger, it acquires an approximately charge-neutral bipolar electrical charge caused by interaction with an ion cloud created by the radioactivity emitted by a capsule containing Krypton-85 (KR-85) gas. The bipolar charged aerosol cloud then enters the region between concentric metal cylinders. An electrostatic potential is established between the cylinders. This arrangement then subjects the charged aerosol particles to the combined forces of aerodynamic drag and electrostatic attraction. An annular strip of small holes is located at the lower end of the hollow center cylinder. At a fixed volumetric flow rate and certain electrostatic potential, a small size range of positively charged particles follows a trajectory that carries them through the holes in the center cylinder, and from there they flow to the output of the DMA. The electrostatic potential can be varied to select the desired size for the particles in the output aerosol. This size range can be varied from 0.01 to 1.0 μm .

In Fig. 9, the DMA was set to produce a particle size of 0.18 μm , and in Fig. 10, the DMA controls were set for a 0.199- μm aerosol particle. Perusal of the tabulated data for both histograms shows that absolutely no counts were noted in the bins for the smallest particle sizes. This observation authenticates the performance of the LAS in the small-particle end of its range. Notice, however, that the LAS values for these two aerosols are 21 percent smaller than those values that were set into the DMA controls. This observation raises the question of the advisability of using Porstendorfer's PSL values for calibration of the LAS.

The presence of multiple-charged large particles is evident in the histograms of Figs. 9 and 10. Except for these particles, the monodispersity of the DMA aerosols is superior to all others yet studied at the ISL or AEDC. On the negative side however, for LDV seeding purposes, existing versions of the DMA are characterized by very low particle-production rates.

2.4 WHISKER PARTICLE CAPTURE SYSTEM

The LAS system is an example of an in-situ aerosol particle sizing scheme where the particles are analyzed while remaining in an airborne state. A notable advantage of the LAS is that the particle size data are available only seconds after an aerosol sample is passed through the instrument. Two disadvantages, however, are associated with light-scattering instruments

like the LAS. The first is the fact that absorptive particles (complex index of refraction) can be undersized. Secondly, all particles, even irregularly shaped ones, are sized in terms of equivalent PSL spheres.

By comparison, the WPC, as well as the electrostatic aerosol sampler described in Section 2.2, is classified as a particle collection device where the particles are removed from the aerosol and subsequently analyzed. The removal techniques include filtration, impaction, or electrostatic deposition. The WPC technique is based on particle deposition upon fine-pored fibrous filters, the so-called whisker collectors, and subsequent electron microscope examination (Ref. 6). The electron microscope examination procedure is time consuming, but as a positive feature, it permits a determination not only of particle size regardless of index-of-refraction, but also particle shape and elemental composition, the latter if an X-ray microanalysis system is added to the electron microscope. This brief comparison of the major features of the LAS and WPC schemes shows that they offer several converse advantages and disadvantages and are, therefore, more complementary than directly competitive for aerosol particle diagnostics.

The whisker particle collector device used in the present study consisted of four collectors housed inside a metal cartridge (Ref. 6). Each collector was a 5-mm-diam bronze grid with a fibrous structure of needle-shaped copper oxide crystals or "whiskers" chemically grown onto the grid wires. The clear area of each grid was 80 by 80 μm . The four collectors were arranged in series inside the cartridge with a spacing of 2.5 mm. The diameters of the copper oxide whiskers typically vary between 0.05 to 0.2 μm with a mean value of 0.1 μm . The number density of whiskers is such that effective filter pore sizes are formed that vary from 1.5 to 5 μm with a typical value of 2.5 μm . The WPC devices were supplied by Opto-Elektronische Instrumente GmbH, Karlsruhe, West Germany (recently merged with TSI, Inc.). A vacuum pump is used to pull aerosol samples through the WPC cartridge with the flow rate adjusted to produce as near isokinetic sampling conditions as possible. An electron micrograph of a whisker collector after particle sampling is shown in Fig. 11.

2.5 AEROSOL SAMPLING EXPERIMENT

The laboratory setup for the aerosol sampling experiment is shown in the diagram of Fig. 12. Particle-free gaseous nitrogen was used with the aerosol generator shown in Fig. 1 to produce the test aerosol. The aerosol was released into a Plexiglas® box with an attached exhaust fan. The flow rate through the WPC was set at 3 ℓ/min by adjustment of a throttling valve. The flow through the EAS was set at 5 ℓ/min . A sample time of 30 to 45 sec was used for the EAS as well as for the WPC.

Two different alumina polishing powders, produced by Union Carbide Corporation of Indianapolis, Indiana, USA, were used in the initial aerosol sampling experiment. The first powder to be tested was the Type C powder with a specified nominal "crystal size" of 1.0 μm . The second powder to be tested was the Type A powder with a specified nominal "crystal size" of 0.3 μm . It should be emphasized at this point that these powders were manufactured for industrial polishing purposes and were in no way optimized for LDV seeding purposes. It was simply that these two powders are widely used for seeding high-temperature flows, and the manufacturer's particle size specifications were considered a good starting point for a comprehensive particle size analysis.

3.0 TEST RESULTS

3.1 EAS RESULTS

Figure 13 is an electron micrograph of a particle sample acquired by the EAS from the Type C 1.0- μm alumina aerosol, but particles and flocs from about 0.2 to about 4 μm can be seen. The exact nature of the floc-bonding mechanisms cannot be discerned from the micrograph, but communications with the powder manufacturer revealed that most of the flocs were probably thermally fused aggregates of primary particles with a lesser number of agglomerates attributable to surface binding forces.

A particle sample captured by the EAS from the Type A 0.3- μm alumina aerosol is shown in Fig. 14. A high percentage of large (> 1.0 μm) flocs are seen. An attempt was made to examine the structure of the flocs by increasing the electron microscope magnification. The magnification for Fig. 14a is 1,000x, whereas that for Fig. 14b is 5,000x, and that for Fig. 14c is 15,000x. In Fig. 14c, the large floc is presumably an aggregate of thermally fused primary particles with maximum dimensions from about 0.1 to about 0.3 μm .

The original plan for the ISL/AEDC particle sizing effort called for particle size distributions to be determined by an AEDC scanning electron microscope (SEM) system. Two EAS samples were set up for automatic particle size analysis. However, the analysis of both samples was terminated before completion because of the excessive amount of time required. The analysis rate was roughly 100 particles/hr, which was much too slow and costly for the anticipated analysis workload. At the AEDC, then, the SEM approach was abandoned in favor of the LAS approach.

3.2 LAS RESULTS

3.2.1 Type C 1.0- μ m Alumina Powder

An aerosol derived from the Type C powder was the first to be analyzed with the LAS. The quick-look histogram for this aerosol is shown in Fig. 15a, and the size distribution is seen to be decidedly polydispersed. The mode of the distribution occurs in the size range from 0.44 to 0.6 μ m, whereas, as will be explained in Section 3.4, the mean diameter was calculated to be 0.93 μ m. This calculated mean diameter is identical, for all practical purposes, to the 1.0- μ m "crystal size" specification of the manufacturer. In its unaltered form, this aerosol is clearly not suitable for general LDV seeding purposes because of the high percentage of large flocs.

3.2.2 Type C 1.0- μ m Alumina with Silica Flow Agent

Several investigators (Refs. 7, 8, and 9) have reported some success in defloccing alumina aerosols by use of a silica flow agent, which is typically blended with the alumina powder as a relatively small mass fraction additive. A flame phase silica product, Cab-O-Sil®, grade EH-5, produced by the Cabot Corporation of Tuscola, Illinois, USA, was cited in Ref. 8 as a beneficial additive. This particular silica product consists of thermally fused aggregate chains of spherical silica particles, which are about 0.007 μ m in diameter. Surface hydroxyl radicals formed during manufacture cause the flame phase silica to be hydrophilic. This particular property of the flow agent accounts for its useful properties as an additive for reducing the tendency of certain foods, pharmaceuticals, and presumably LDV seeding materials to form agglomerates.

One model proposed by the Cabot Corporation (Ref. 10) has the silica aggregates adhering to the surface of larger primary particles (e.g. alumina particles). Surface bonding forces in this case occur between the silica aggregates and the primary particles rather than between primary particles. This effectively allows the primary particles to exist in close proximity without forming agglomerates. This model proposes a mechanism for suppression of the propensity to form agglomerates, but proposes no mechanism for reduction of alumina aggregates into primary particles.

A mixture of the Type C 1.0- μ m powder and 0.5 percent by weight of the silica flow agent was prepared at the AEDC and tested. The LAS size spectrum for the resultant aerosol is shown in Fig. 15b. It can be seen that the flow agent has helped very little; the only noticeable effect is an increase in the percentage of small particles.

Further observations involving the silica flow agent showed that as its mass fraction was increased above the 0.5-percent range, it actually seemed to promote macroscopic agglomeration since a significant increase in nitrogen flow rate through the aerosol generator was necessary to maintain a reasonable particle number density in the output aerosol. This observation is consistent with the Cabot Corporation (Ref. 10) descriptions of the silica aggregates forming hydroxyl-to-hydroxal radical bonds when present in a mixture in sufficient quantity. As the silica mass fraction is increased, the hydroxal bonds eventually form cohesive matrices in the mixture that tend to bond macroscopic volumes of the mixture together.

The Cabot Corporation literature suggests that low-energy mixing techniques be employed to blend the Cab-O-Sil with the host powder. Low-energy blending is necessary to maintain the integrity of the chainlike silica aggregates. At the AEDC, the mixing process was accomplished by tumbling the Cab-O-Sil and alumina powder together in a lapidary tumbler. Since the AEDC experience with the flow agent was not positive, questions arose as to the adequacy of the blending process. For this reason it was decided that a commercially available alumina-powder/silica-flow-agent product should be purchased and tested.

3.2.3 Proprietary Alumina/Silica Powder

A proprietary mixture of nominal 0.7- μm aluminum-oxide powder and silica flow agent was purchased from Micro Abrasives Corporation of Westfield, Massachusetts, USA. The LAS spectrum for the aerosol derived from this product is shown in Fig. 15c, and it is seen to be virtually identical to the spectrum of Fig. 15a.

These observations showed that the silica flow agent was, at best, marginally useful for defloccing the alumina polishing powder. At this point in the study, it was concluded that the flocs were predominantly firmly bound aggregates and that other approaches should be investigated for producing an improved solid-particle aerosol, such as seeking powders with a better intrinsic particle size characteristic, the use of energetic defloccing techniques, the use of size classification techniques or some combination of these approaches.

3.2.4 Deagglomeration by Sonic Orifice

Marteney (Ref. 11) has described an aerosol dispensing nozzle with near-sonic conditions in the nozzle passage that was shown to be useful for breaking up agglomerates in solid-particle aerosols. Morrisette and Bushnell (Ref. 12) have also reported the use of sonic flow in an array of 25- by 300- μm slits in the wall of a tube for breaking up agglomerates in solid-particle aerosols.

A simple, circular, sonic orifice with a diameter of 1.0 mm was evaluated at the AEDC for defloccing aerosols derived from the Type C 1.0- μm alumina powder. The LAS spectrum is shown in Fig. 15d. Comparison of this size spectrum with that of Fig. 15a shows some reduction in the percentage of large flocs with an attendant increase in the percentage of small particles.

3.2.5 Super Finish and Agglomerate-Free Alumina Powders

The Super Finish (SF) and Agglomerate-Free (AF) alumina powders are relatively new polishing powder products offered by Union Carbide Corporation. Agglomerates in these two products are supposed to be more easily crushed than those in regular polishing powder under the typical mechanical pressures exerted during a surface polishing operation. Test quantities of these powders were acquired for evaluation on the chance that they might also exhibit a lessened tendency to produce agglomerates in their aerosols.

The particle size histogram for the 1.0- μm AF alumina powder is shown in Fig. 15e, and the histogram for the same aerosol after deagglomeration by the sonic orifice is shown in Fig. 15f. The sonic orifice was only marginally effective in reducing the percentage of large flocs.

Obviously, the AF alumina aerosol is not much better than that derived from the Type C powder for LDV seeding purposes. The 1.0- μm SF alumina powder was not tested, but the 0.3- μm SF and AF powders were tested and somewhat unexpected results were observed as described in Section 3.2.7.

3.2.6 Type A 0.3- μm Alumina Powder

Aerosols derived from the Union Carbide Type A 0.3- μm alumina powder with and without the sonic orifice were analyzed by the LAS. In Fig. 16a, as might be expected, the particle size spectrum for the Type A aerosol is seen to have less large-particle content than any of the previously examined 1.0- μm alumina aerosols. Also, a significant portion of the aerosol particle population at the small-particle end of the spectrum is undoubtedly not being accounted for because of the lower size-detection limit of the LAS. This suspicion is substantiated by the high-resolution spectrum shown in Fig. 16b. The trend of increasing bin counts as particle size decreases suggests that there are probably significant numbers of particles in the aerosol that are smaller than 0.09 μm . This is of concern for LDV seeding considerations since particles smaller than the LDV system detection limit cannot contribute to the generation of useful LDV signals, but can contribute to the background noise level. It is informative to note that the mean value of the distribution in Fig. 16a is 0.3 μm , which is exactly the nominal size specification quoted by the powder manufacturer.

The sonic orifice produces a noticeable decrease in the percentage of large agglomerates as shown in Fig. 16c. At this point in the study, the remaining large-particle content was assumed to consist of aggregates of firmly bound primary particles. Aggregate breakup schemes involving more energy than the simple sonic orifice approach were considered necessary if further reduction in the large-particle content was to be realized. Schemes involving additive flow agents were not pursued further since aggregate breakup appeared to be the main problem rather than suppression of agglomerate formation in the bulk powder.

3.2.7 SF and AF 0.3- μm Alumina Powders

The manufacturer's literature indicates that the SF and AF polishing powder products are the result of special milling and size classification processes that reduce the aggregates to individual polishing crystals. Intuitively, it seems reasonable that these processes would also yield a superior powder from which to generate an LDV seed aerosol. However, this was not found to be the case as illustrated by the SF size spectrum in Fig. 16d. The mode value of the histogram is in the desirable size range ($\sim 0.2 \mu\text{m}$) for a seed aerosol, but the large-particle content is surprisingly worse than the Type A powder.

The AF 0.3- μm alumina powder produces an aerosol with particle size characteristics similar to that of the SF powder as shown in Fig. 16e. Partial defloccing with the sonic orifice improves the size spectrum somewhat as shown in Fig. 16f, but this aerosol is still inferior to the one derived from the Type A powder.

It is obvious that the AEDC goal of developing a technique to thoroughly defloc the 0.3- and 1.0- μm alumina aerosols was not attained. As far as the mutual ISL/AEDC goal of developing an improved solid-particle seeding technique for high-temperature flows is concerned, it seems advisable to search for an aggregate-free powder or to develop a size classification scheme to separate the desired range of particle sizes from the polydispersed aerosols.

3.3 WPC RESULTS

In order to establish the size distribution of the particle samples, photographically enlarged micrographs of the whisker collectors, as shown in Figs. 17 and 18, were processed by a semiautomatic particle size analyzer (Ref. 6). This instrument allows the physical size of captured particles to be classified into 48 intervals on either a linear or a logarithmic scale. The resultant size data can be displayed in a histogram format or as cumulative number distributions.

The total size range covered by the particle size analyzer depends on the final magnification of the micrographs; it was chosen to be 0.04 to 0.92 μm , in the present case, according to a preliminary check of the size distribution.

Each of the four collectors forming one whisker filter assembly has been processed separately since additional information on the transfer characteristics of the whisker filters was expected from comparing the size distributions on successive collectors. The resultant histograms for the Type C 1.0- μm and the Type A 0.3- μm alumina samples are shown in Figs. 19 and 20, respectively. In these figures as well as in the following ones, only the first and last collector of each assembly are considered for the purpose of presentation clarity. As stated in Section 1.3, the data reduction procedure at ISL was based on the premise that flocs observed in the micrographs were caused by agglomeration of prime particles as they impinged upon the copper oxide whiskers. Based on this premise, then, the recognizable prime particles in a magnified floc image were visually identified and counted as so many prime particles with certain sizes rather than as one large floc particle.

For the 0.3- μm alumina powder, only little change is observed between the size distributions on the different collectors, whereas in the case of the 1.0- μm alumina powder the distribution on the last collector is clearly shifted towards smaller particle diameters. A size shift as in the latter case is predicted from the theory of aerosol filtration by fibrous filters (Ref. 13) and has already been found in comparable situations where direct interception is the predominant mechanism of collection (Ref. 6).

The measurement results can be expressed in a more quantitative way if the empirical size distribution is represented by an analytical function. As demonstrated in Fig. 21, successful modeling of the experimental data may be done using a log-normal distribution. In the case of log-normally distributed particle sizes, the probability density function, p , of the particle diameter, D , is determined by two characteristic constants, the median, c , and the geometric standard deviation, s , according to the relation

$$p(D) = \frac{1}{D \cdot \ln s \cdot \sqrt{2\pi}} \exp \left[-\frac{1}{2} \left(\frac{\ln D - \ln c}{\ln s} \right)^2 \right] \quad (1)$$

The mode m and the mean diameter \bar{D} of the log-normal distribution can also be expressed in terms of the parameters c and s ,

$$m = c \cdot \exp[-(\ln s)^2] \quad (2)$$

$$\bar{D} = c \cdot \exp \frac{1}{2} (\ln s)^2 \quad (3)$$

To verify whether an empirical distribution is log-normal, it is convenient to plot the cumulative percentage distribution on log-probability paper. If a straight line is obtained, the distribution can be considered as log-normal. Another useful property of the log-probability plot is that

it allows the parameters c and s (See Fig. 21) to be determined graphically (Ref. 14). The log-probability plots for the Type C 1.0- μm and the Type A 0.3- μm alumina powder samples together with the results of curve fitting are shown in Figs. 22 and Fig. 23, respectively.

Knowing the particle size distribution on successive stages of a whisker collector assembly, one is able to determine the collection efficiency of the filters as a function of particle diameter. As has been found earlier (Ref. 6), the efficiency of whisker collectors for particles in the submicron range can be approximated by an exponential function of the type $\eta = 1 - \exp(-\alpha \cdot D)$, where D is the particle diameter, and α is the coefficient of absorption that is only dependent upon collector properties. The values resulting from the present analysis are $\alpha \leq 0.5/\mu\text{m}$ in the case of the 0.3- μm alumina sample, and $\alpha = 2.7/\mu\text{m}$ in the case of the 1.0- μm alumina sample. The coefficient of absorption inferred from the 0.3- μm sample is considerably smaller than can be explained by the theory of filtration. This may have been caused by an inadequate capability to visually study the micrographs and thereby detect and account for the very small ($\sim 0.1 \mu\text{m}$) constituents of the flocs. The empirical collection efficiency derived from the whisker collector analysis can be used in a data reduction algorithm for the inversion of the measurement results (Ref. 6) to obtain the original size distribution of the aerosol (Figs. 24 and 25).

3.4 COMPARISON OF WPC AND LAS RESULTS

It is now clear that the predominant percentage of flocs observed at the ISL and AEDC were originally present in the aerosol rather than being formed during the aerosol sampling process. This is not to say that agglomeration did not occur in the WPC since agglomeration definitely will occur if a large enough number of aerosol particles are drawn through the WPC. The point to be made is that the WPC analysis scheme cannot differentiate between flocs originally existing in the aerosol and agglomerates formed during the aerosol sampling process. The LAS, on the other hand, can directly detect large and small aerosol particles on-line and in-situ, but cannot differentiate large primary particles from similarly sized flocs.

This set of circumstances precluded a direct comparison of particle size spectra from the two systems in order to certify one system with respect to the other. However, useful information can still be gained by comparing the particle size information from the WPC, the LAS, and the powder manufacturer.

Because of the two different ways of treating flocs, it is expected that an LAS histogram will be skewed to the large-particle end of the size spectrum with respect to a WPC histogram anytime that aerosol flocs are encountered. This effect can clearly be seen by a cursory comparison of Figs. 15a and 19, whereas the effect is not quite so obvious when Fig. 16a is compared with Fig. 20.

A more detailed comparison of the WPC and LAS results, however, can only be carried out on the basis of the probability density functions instead of on the basis of histograms. Moreover, the final (i.e. the inverted) WPC size distribution should be used for comparison with the LAS results since it has been corrected for the nonuniform collection efficiency of the whisker collectors.

Continuing the comparison process, a log-normal function was fitted to both the WPC and LAS data for the Type C and Type A alumina powder aerosols as shown in Figs. 24 and 25. The associated size statistics are provided in Table 1. It can be seen that the mean particle diameters as determined by the LAS for the 0.3- μm alumina aerosol (LAS mean, 0.40 μm) and the 1.0- μm alumina aerosol (LAS mean, 0.88 μm) are in good agreement with the powder manufacturer's nominal particle size specifications. However, it is somewhat disconcerting to view this agreement in light of the fact that both the 0.3- μm and 1.0- μm alumina aerosols undoubtedly contain significant numbers of particles below the small-particle detection limit of the LAS (See Section 3.2.6). If these very small ($< 0.09 \mu\text{m}$) particles could be detected and taken into account, the mean particle size for both aerosols would surely shift toward smaller values. With regard to the good agreement then, it seems that the LAS and the powder manufacturer's particle sizing instrument must have had similar small-particle detection limits. At the time of this study, a detailed description of the technique used to determine the crystal size (nominal particle size) for the two alumina powders was not available from the powder manufacturer.

For the 0.3- μm aerosol as well as for the 1.0- μm aerosol, the width of the WPC size distribution is considerably smaller than the width derived from the LAS measurements ($s = 1.30$ compared to 2.2, and $s = 1.28$ compared to 1.9, respectively). Consequently, the mode, median, and mean diameter resulting from the WPC data are nearly equal quantities, whereas the respective values differ clearly in the case of the LAS results. This might be expected because of the different way of treating flocs, which, in the WPC scheme, were not sized as individuals, but rather were dissected analytically into primary particles. Nevertheless, the mode values of the WPC and LAS distribution are in excellent agreement for the 1.0- μm aerosol. In the case of the 0.3- μm powder aerosol, however, the mode value derived from the WPC measurements is nearly twice as large as that resulting from the LAS data. This can only be explained by an insufficient dissection of agglomerates when analyzing the WPC micrographs.

4.0 OBSERVATIONS, SUMMARY OF RESULTS, AND CONCLUSIONS

As a result of the joint ISL/AEDC aerosol particle sizing experiment, the WPC and LAS techniques were found to be more complementary than directly competitive. For example, the WPC could not distinguish between flocs originally present in the test aerosol and those

formed during the aerosol particle capture process. By comparison, the LAS could resolve the floc origination question but could not distinguish between large primary particles and similarly sized flocs composed of smaller primary particles. Further, the WPC is capable inherently of providing particle shape information, whereas the LAS sizes all primary particles and flocs in terms of equivalent PSL spheres. Moreover, elemental composition of the aerosol particles can be determined by an X-ray unit attached to the basic WPC system, whereas no such information is available with the LAS.

The aerosol particle size information from the LAS is electronically processed, and the data are available on-line within several minutes after the aerosol is sampled. By contrast, the WPC particle size data are produced off-line after several hours of electron microscope analysis. The WPC is particularly well suited for conveniently capturing field samples of an aerosol and then performing the particle size analysis in the laboratory at a later time. This is because the entire WPC particle-capture mechanism can be simply and easily carried and operated by one person. Also, once the aerosol particles are captured, their particle size distribution does not change with time.

The LAS system, on the other hand, is a laboratory instrument weighing about 100 kg. Furthermore, the LAS aerosol samples, unlike the captured WPC samples, must be processed immediately since the aerosol particle size distribution characteristic changes with time because of sedimentation and diffusion losses to the inside surface of the plastic aerosol sample bag (See Fig. 3).

The accuracy of the LAS was certified by comparing its measurements with aerosols containing known sizes of PSL spheres. A DMA device was used to double-check the performance of the LAS in the size range below $0.3\ \mu\text{m}$. The LAS was found to perform in a reasonable fashion in this size range. Measurements by the certified LAS were then compared to measurements by the WPC, and it was found that the premise for analyzing the WPC micrographs was not properly chosen for aerosol particles in the size range below $0.3\ \mu\text{m}$. Also, the misinterpretation of flocs in the WPC samples was found to be responsible for an underestimation of the large-particle content of an aerosol containing flocs.

Two different aerosols derived from alumina powders with manufacturer's nominal size ("crystal size") specifications of 0.3 and $1.0\ \mu\text{m}$ were used as test aerosols for the WPC and LAS. Both these aerosols were found to be polydispersed, and each included a range of primary particle sizes from below the lower limit of the LAS ($0.09\ \mu\text{m}$) up to the vicinity of the manufacturer's specified nominal size. An appreciable percentage of flocs larger than the nominal size was also observed in each aerosol. The predominant percentage of these flocs was thought to be thermally fused aggregates of primary particles. Because the flocs were aggregates or at least very firmly bound agglomerates, the use of a silica flow agent was,

at best, marginally useful in reducing the percentage of flocs in the two aerosols. For the same reasons, the use of the sonic orifice approach for deagglomeration of the alumina aerosols was only marginally effective in reducing the percentage of aerosol flocs.

Two relatively new alumina polishing powder products, the SF and AF line of powders, were evaluated as possible source material for a suitable seed particle aerosol. These powders are specially milled during manufacture to break up aggregates. It was assumed that a reduced aggregate content would result in improved aerosol particle size characteristics compared to the ordinary type of polishing powder. Surprisingly, however, the SF and AF aerosols actually contained a higher percentage of large flocs than aerosols derived from the ordinary powder. A DMA device was used during the certification procedure for the LAS. This type of aerosol generator was found to produce a very narrow particle size distribution and would be a useful seed aerosol generator except for its low particle-production rate.

REFERENCES

1. Crosswy, F. L. "Particle Size Distributions of Several Commonly Used Seeding Aerosols." *Wind Tunnel Seeding Systems for Laser Velocimeters*, NASA Conference Publication 2393, March 19-20, 1985.
2. Yamada, Y., Miyamoto, K., and Koizumi, A. "Size Measurement of Latex Particles by Laser Aerosol Spectrometer." *Aerosol Science and Technology*, Vol. 5, 1986, pp. 377-384.
3. Hodgkinson, J. R. "The Optical Measurement of Aerosols." *Aerosol Science*, Edited by C. N. Davies, Academic Press, New York, 1966.
4. Heard, M. J., Wells, A. C., and Wiffen, R. D. "A Re-Determination of the Diameters of DOW Polystyrene Latex Spheres." *Atmospheric Environment*, Vol. 4, 1970, pp. 149-156.
5. Porstendorfer, J. and Heyder, J. "Size Distributions of Latex Particles." *Journal of Aerosol Science*, Vol. 3, 1972, pp. 141-148.
6. Schafer, H. J. and Pfeifer, H. J. "Deduction of Aerosol Size Distribution from Particle Sampling by Whisker Collectors." *Experiments in Fluids*, Vol. 1, 1983, pp. 185-193.
7. Meadows, D. M. et al. "Laser Velocimeter for Supersonic Jet Turbulence and Turbulence Spectra Research." Appendix IV of The Generation and Radiation of Supersonic Jet Exhaust Noise, AFAPL-TR-74-24, June 1974.

8. Patrick, W. P. and Paterson, R. W. "Velocimetry Measurements in Strongly Accelerated Nozzle Flow Fields." AIAA 14th Fluid and Plasma Dynamics Conference, AIAA-81-1198, June 1981.
9. Koch, H. W. et al. "Messungen mit dem Elektrischen Aerosol Analysator der Firma Thermo-Systems, Inc. (TSI) und Vergleich mit der Whiakernetz-Methode." Note N 612/76, ISL Saint Louis, France.
10. Cabot Corporation. "Cab-O-Sil Properties and Functions." Cab-O-Sil Division, Box 188, Tuscola, Illinois 61953.
11. Martenay, P. J. "Experimental Investigation of the Opacity of Small Particles." NASA CR-211, April 1965.
12. Morrisette, E. L. and Bushnell, D. M. "Powder Fed Sheared Dispersal Particle Generator." U. S. Patent No. 4,428,703, August 28, 1981.
13. Pich, J. "Theory of Aerosol Filtration by Fibrous and Membrane Filters." *Aerosol Science*. Academic Press, London-New York, 1966.
14. Allen, T. *Particle Size Measurement*. Chapman and Hall Ltd., London 1968.

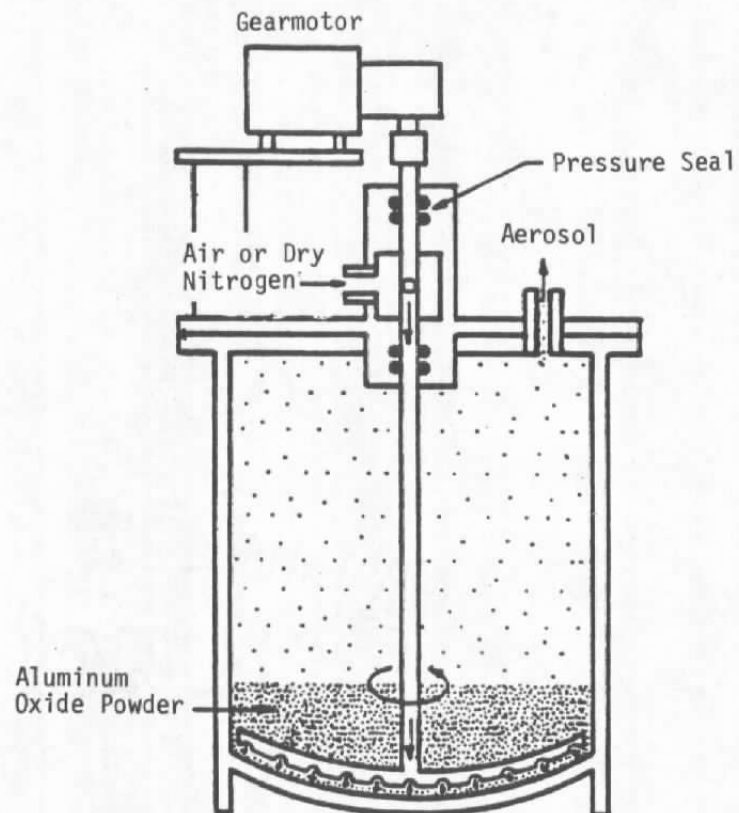


Figure 1. Mechanically agitated, fluidized bed seeder.

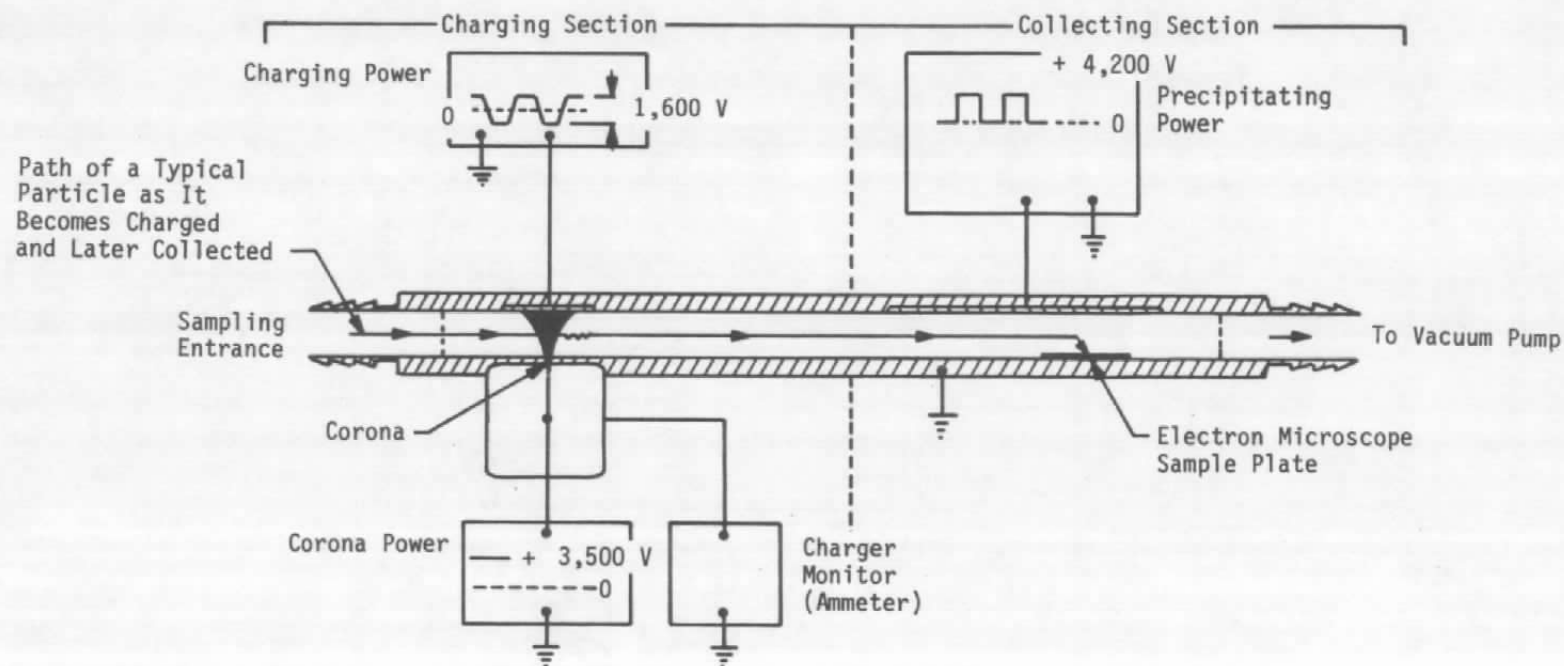


Figure 2. Electrostatic aerosol sampler (EAS).

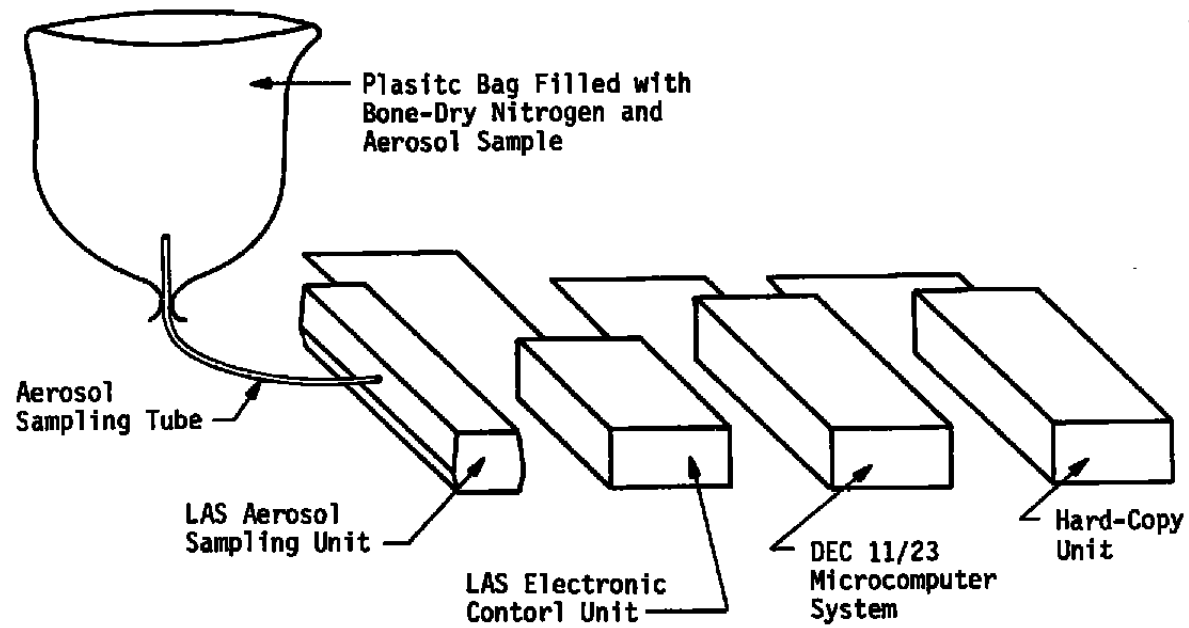


Figure 3. Laser aerosol spectrometer (LAS) system.

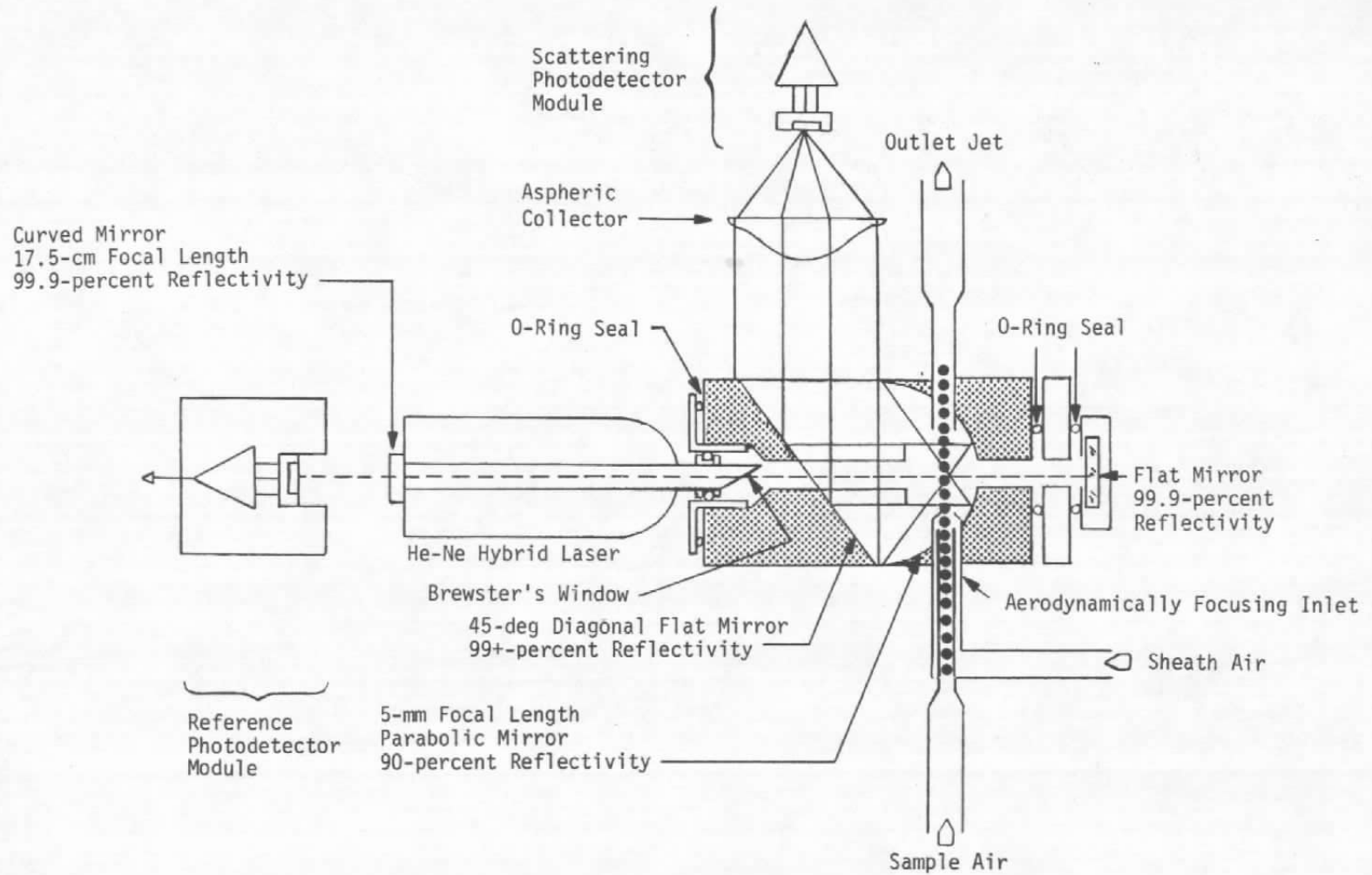
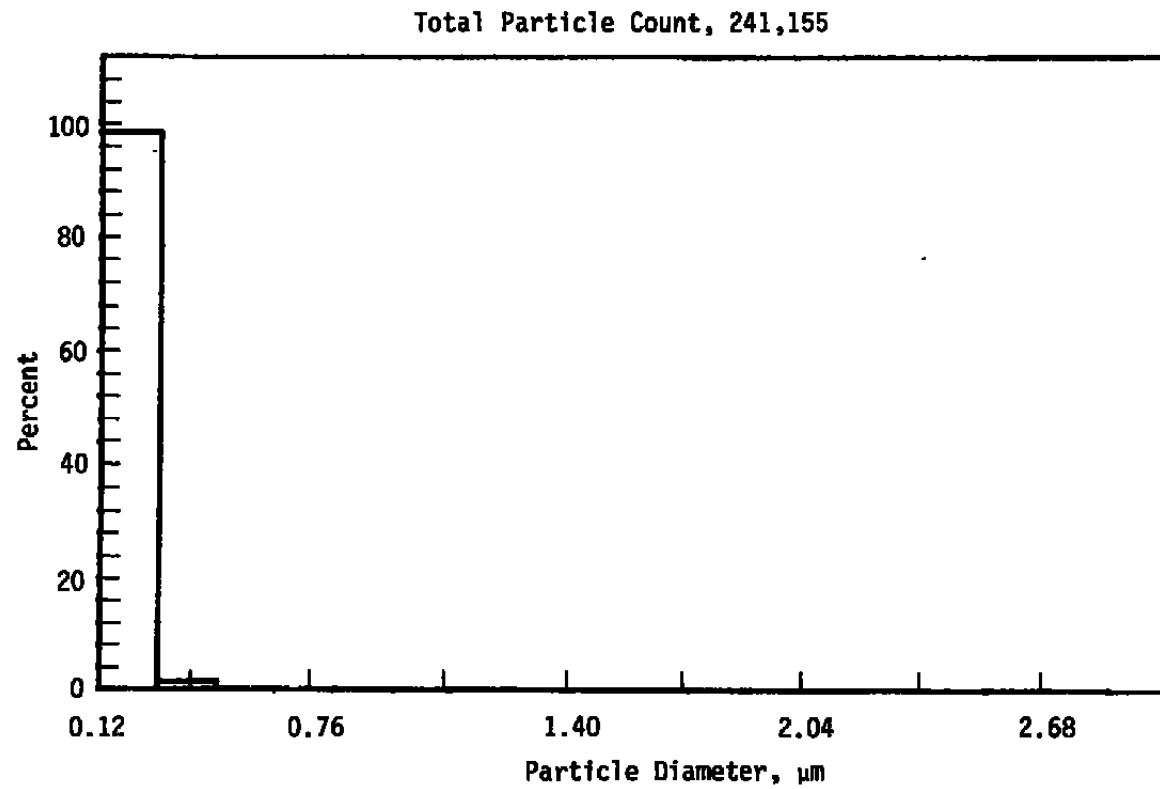
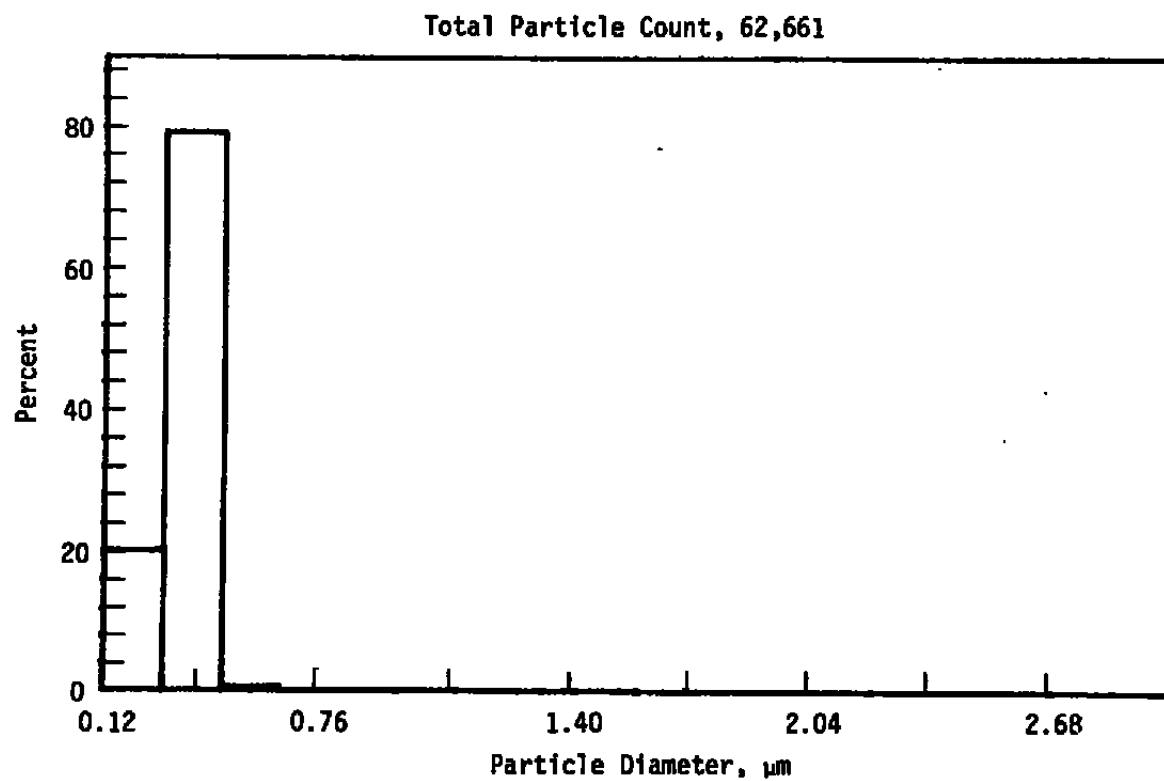


Figure 4. Laser optics for the LAS.

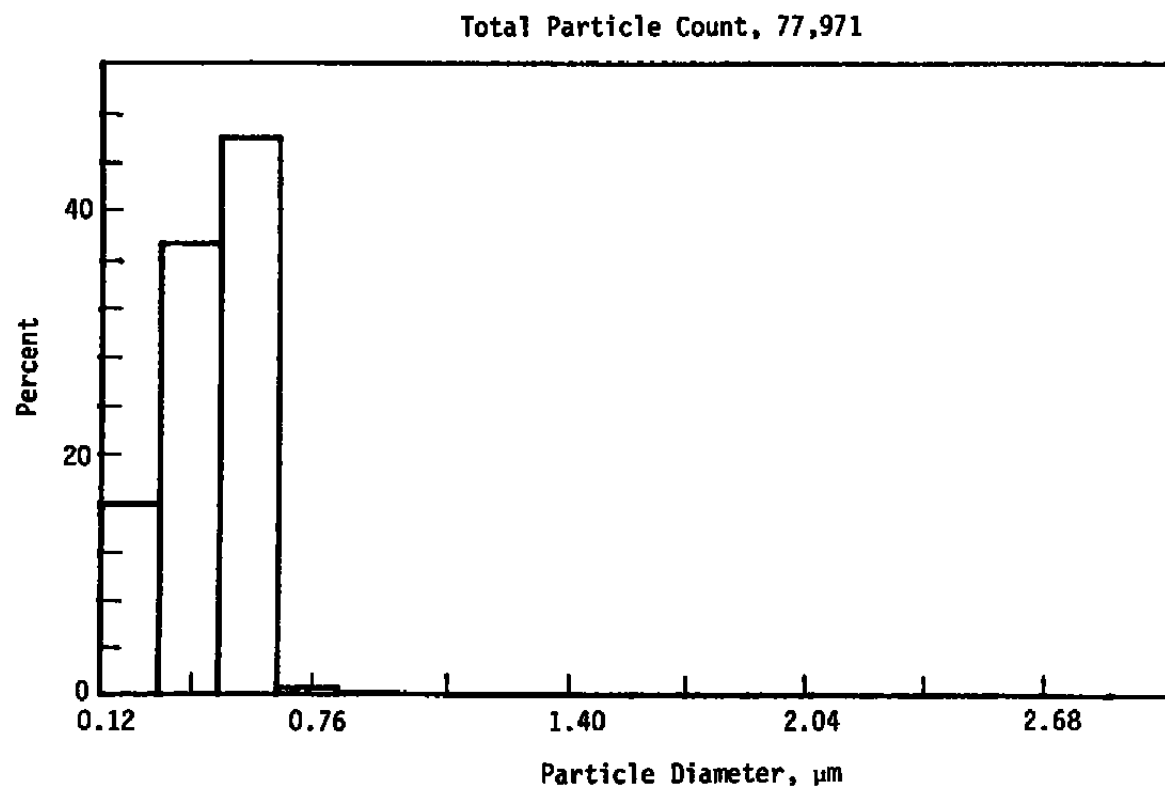


a. 0.176- μm PSL spheres

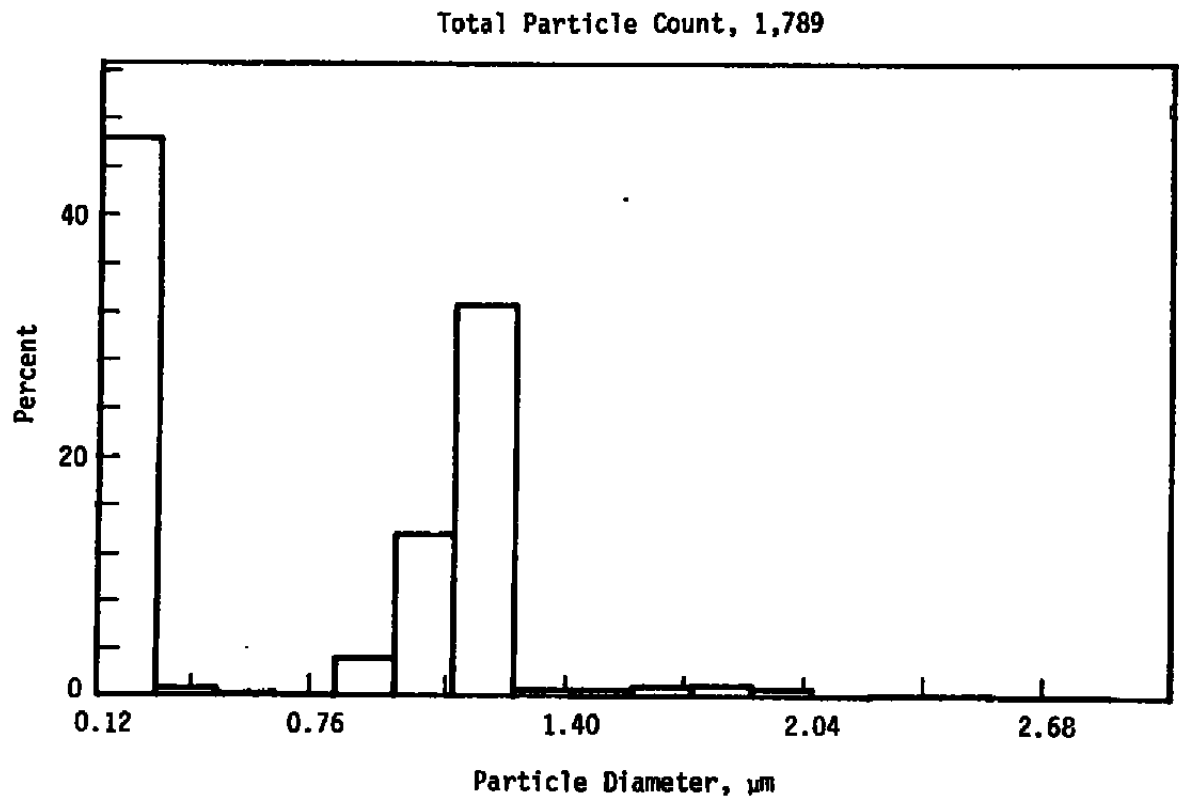
Figure 5. Quick-look histograms for the five certification aerosols.



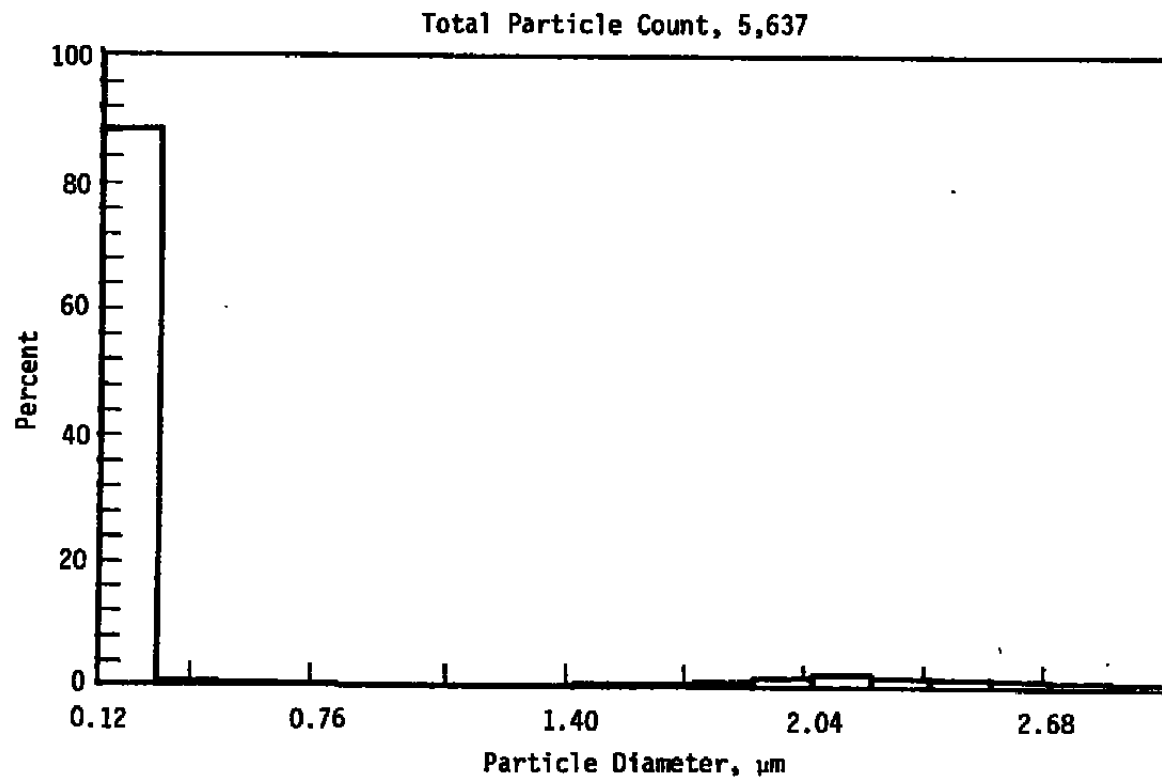
b. 0.312- μm PSL spheres
Figure 5. Continued.



c. 0.497- μm PSL spheres
Figure 5. Continued.



d. 1.091- μm PSL spheres
Figure 5. Continued.



e. 2.02- μm PSL spheres
Figure 5. Concluded.

Total Particle Count, 195,045

<u>Bin</u>	<u>Count</u>	<u>Percent</u>	<u>Size/μm</u>
1	211	0.108180	0.090 to 0.097
2	208	0.106642	0.097 to 0.104
3	232	0.118947	0.104 to 0.111
4	451	0.231229	0.111 to 0.118
5	1,633	0.837243	0.118 to 0.125
6	5,832	2.990080	0.125 to 0.132
7	16,662	8.542640	0.132 to 0.139
8	45,052	23.098300	0.139 to 0.146
9	63,109	32.356100	0.146 to 0.153
10	15,148	7.766410	0.153 to 0.160
11	5,092	2.610680	0.160 to 0.167
12	7,897	4.048810	0.167 to 0.174
13	11,061	5.671000	0.174 to 0.181
14	11,753	6.025790	0.181 to 0.188
15	10,704	5.487960	0.188 to 0.195

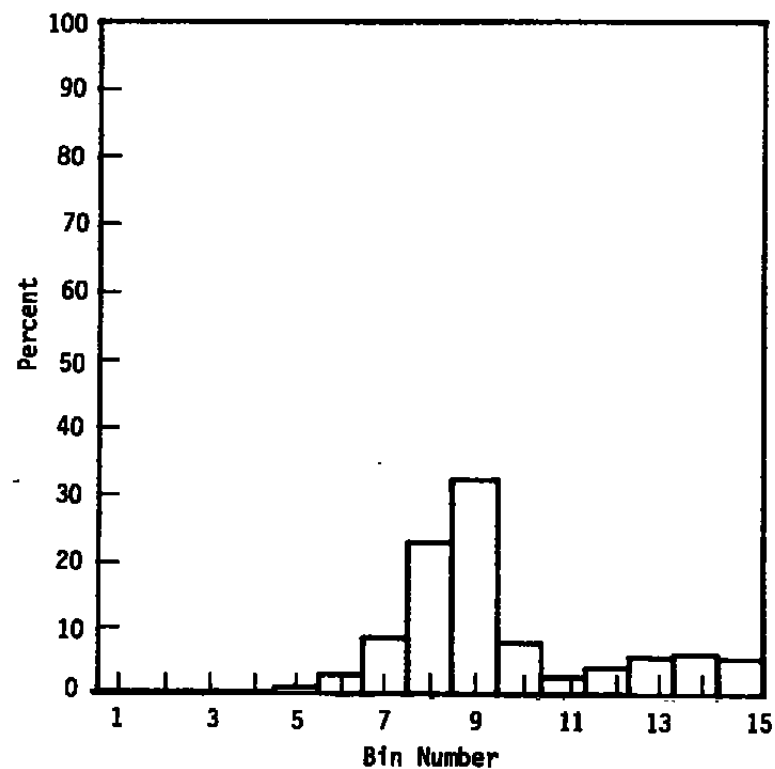
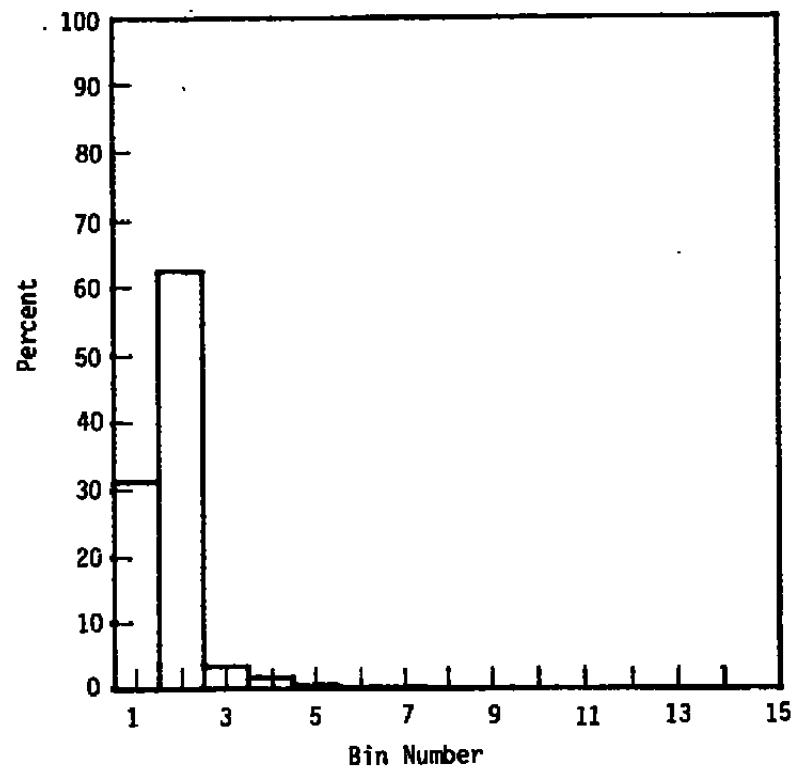
a. 0.176- μm PSL spheres

Figure 6. High-resolution histograms for the five certification aerosols.

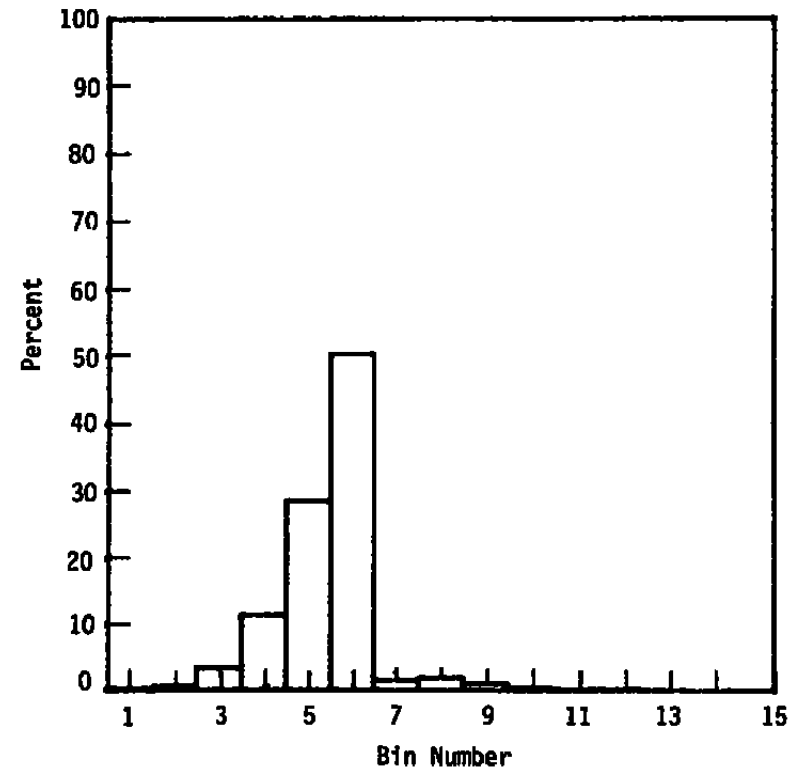
Total Particle Count, 72,657

<u>Bin</u>	<u>Count</u>	<u>Percent</u>	<u>Size/μm</u>
1	22,731	31.28540000	0.24 to 0.28
2	45,433	62.53080000	0.28 to 0.32
3	2,551	3.51102000	0.32 to 0.36
4	1,251	1.72179000	0.36 to 0.40
5	371	0.51061800	0.40 to 0.44
6	160	0.22021300	0.44 to 0.48
7	67	0.09221410	0.48 to 0.52
8	40	0.05505320	0.52 to 0.56
9	13	0.01789230	0.56 to 0.60
10	7	0.00963431	0.60 to 0.64
11	5	0.00688165	0.64 to 0.68
12	9	0.01238700	0.68 to 0.72
13	11	0.01513960	0.72 to 0.76
14	5	0.00688165	0.76 to 0.80
15	3	0.00412899	0.80 to 0.84



b. 0.312- μ m PSL spheres
Figure 6. Continued.

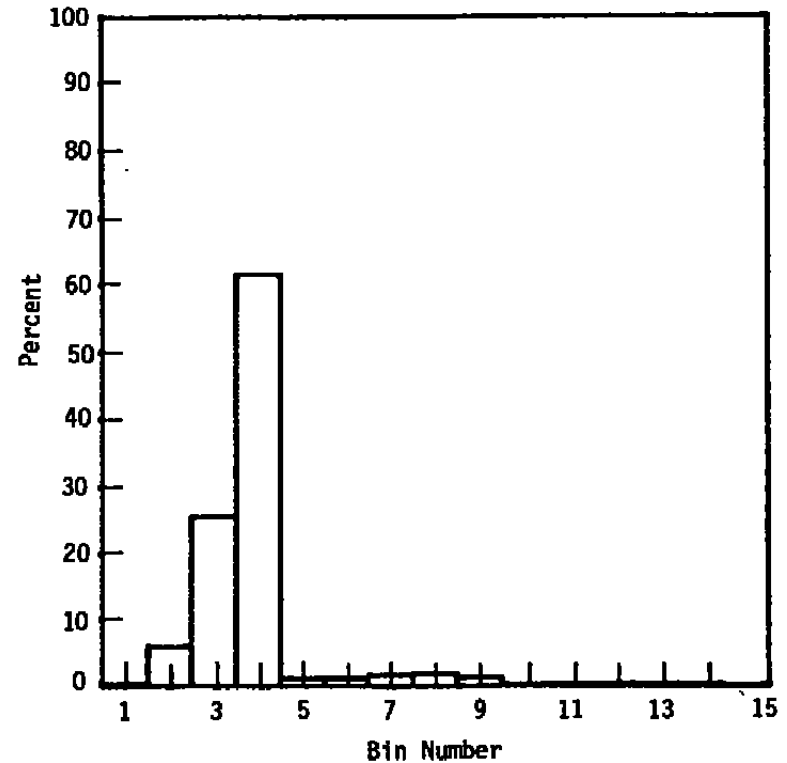
<u>Bin</u>	<u>Count</u>	<u>Percent</u>	<u>Size/μm</u>	
1	101	0.1538410	0.24	to 0.28
2	403	0.6138430	0.28	to 0.32
3	2,286	3.4820000	0.32	to 0.36
4	7,556	11.5092000	0.36	to 0.40
5	18,918	28.8156000	0.40	to 0.44
6	33,122	50.4509000	0.44	to 0.48
7	1,002	1.5262300	0.48	to 0.52
8	1,152	1.7547100	0.52	to 0.56
9	640	0.9748370	0.56	to 0.60
10	228	0.3472860	0.60	to 0.64
11	98	0.1492720	0.64	to 0.68
12	77	0.1172850	0.68	to 0.72
13	35	0.0533114	0.72	to 0.76
14	21	0.0319868	0.76	to 0.80
15	13	0.0198014	0.80	to 0.84



c. 0.497- μm PSL spheres
Figure 6. Continued.

Total Particle Count, 947

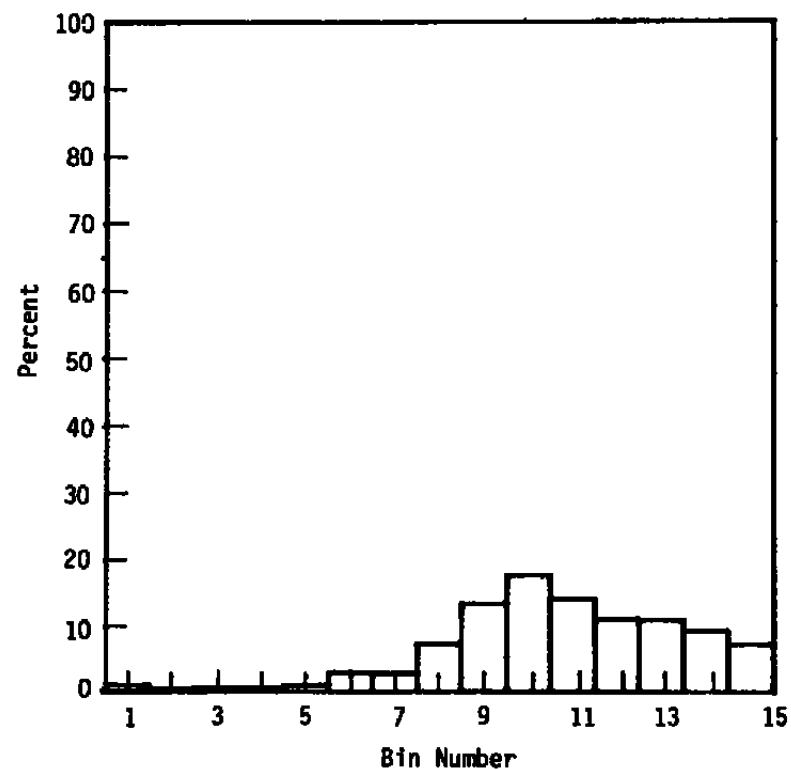
<u>Bin</u>	<u>Count</u>	<u>Percent</u>	<u>Size/μm</u>
1	1	0.105597	0.60 to 0.76
2	57	6.019010	0.76 to 0.92
3	244	25.765600	0.92 to 1.08
4	583	61.562800	1.08 to 1.24
5	8	0.844773	1.24 to 1.40
6	9	0.950370	1.40 to 1.56
7	14	1.478350	1.56 to 1.72
8	15	1.583950	1.72 to 1.88
9	10	1.055970	1.88 to 2.04
10	0	0.000000	2.04 to 2.20
11	1	0.105597	2.20 to 2.36
12	2	0.211193	2.36 to 2.52
13	2	0.211193	2.52 to 2.68
14	1	0.105597	2.68 to 2.84
15	0	0.000000	2.84 to 3.00



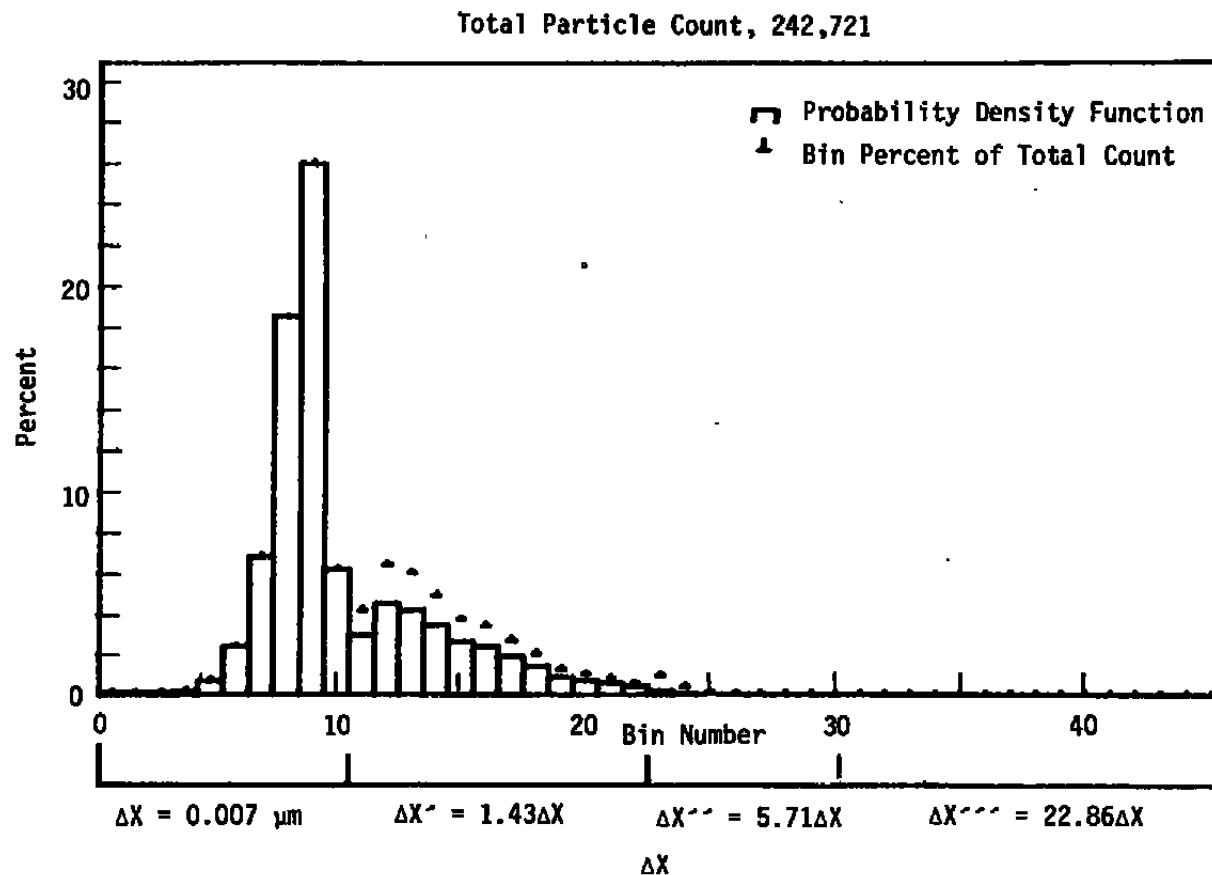
d. 1.091- μm PSL spheres
Figure 6. Continued.

Total Particle Count, 609

<u>Bin</u>	<u>Count</u>	<u>Percent</u>	<u>Size/μm</u>	
1	6	0.985222	0.60	to 0.76
2	2	0.328407	0.76	to 0.92
3	3	0.492611	0.92	to 1.08
4	3	0.492611	1.08	to 1.24
5	5	0.821018	1.24	to 1.40
6	18	2.955670	1.40	to 1.56
7	17	2.791460	1.56	to 1.72
8	44	7.224960	1.72	to 1.88
9	82	13.464700	1.88	to 2.04
10	109	17.898200	2.04	to 2.20
11	86	14.121500	2.20	to 2.36
12	68	11.165800	2.36	to 2.52
13	66	10.837400	2.52	to 2.68
14	56	9.195400	2.68	to 2.84
15	44	7.224960	2.84	to 3.00



e. 2.02- μ m PSL spheres
Figure 6. Concluded.

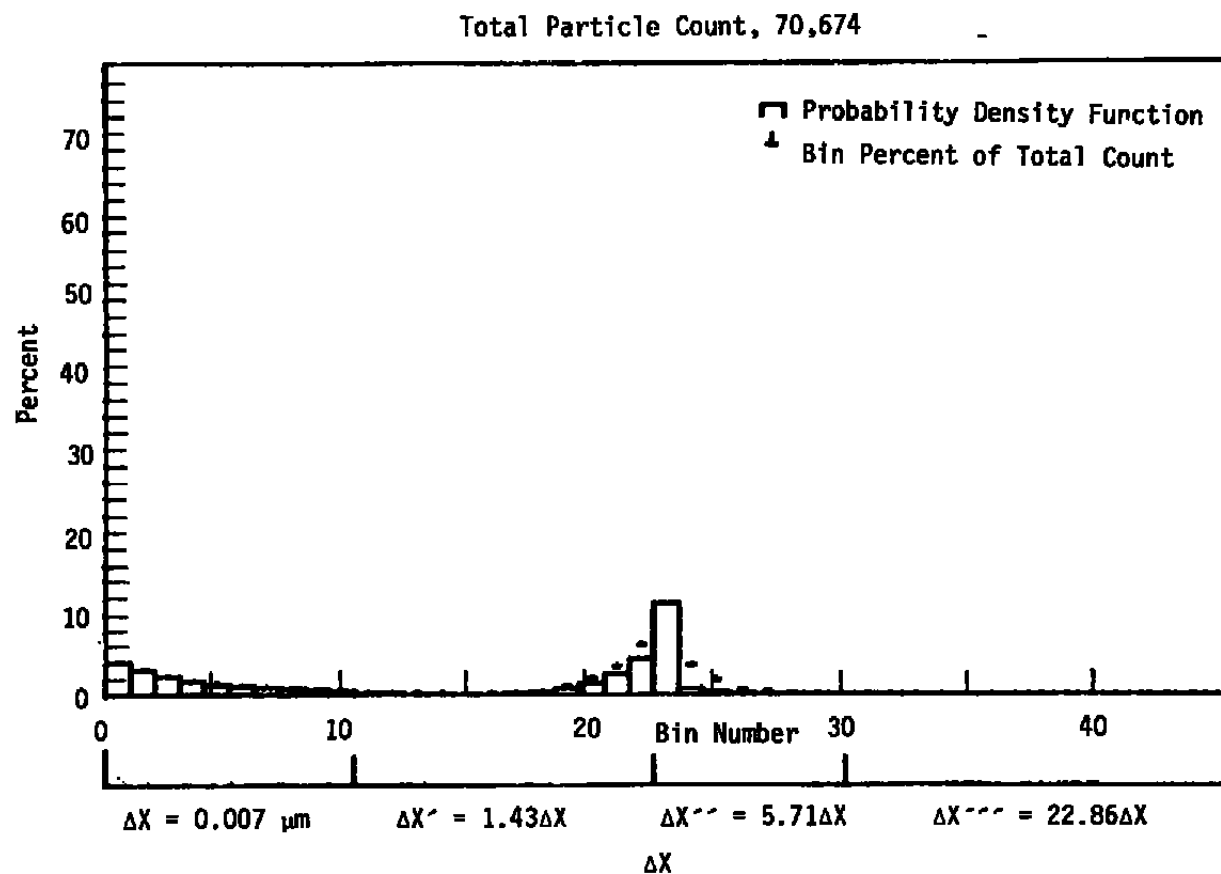


a. 0.176- μm PSL spheres

Figure 7. High-resolution composite histograms for the five certification aerosols.

<u>Bin</u>	<u>Count</u>	<u>Percent</u>	<u>Size/μm</u>	<u>Bin</u>	<u>Count</u>	<u>Percent</u>	<u>Size/μm</u>
1	211	0.08693110	0.090 to 0.097	24	967	0.398400000	0.32 to 0.36
2	208	0.08569510	0.097 to 0.104	25	205	0.084459100	0.36 to 0.40
3	232	0.09558300	0.104 to 0.111	26	93	0.383156000	0.40 to 0.44
4	451	0.18581000	0.111 to 0.118	27	52	0.021423800	0.44 to 0.48
5	1,633	0.67278900	0.118 to 0.125	28	23	0.009475900	0.48 to 0.52
6	5,832	2.40276000	0.125 to 0.132	29	21	0.008651910	0.52 to 0.56
7	16,662	6.86467000	0.132 to 0.139	30	15	0.006179930	0.56 to 0.60
8	45,052	18.56120000	0.139 to 0.146	31	18	0.007415920	0.60 to 0.76
9	63,109	26.00060000	0.146 to 0.153	32	12	0.004943950	0.76 to 0.92
10	15,148	6.24091000	0.153 to 0.160	33	8	0.003295970	0.92 to 1.08
11	10,256	4.22543000	0.160 to 0.170	34	2	0.000823991	1.08 to 1.24
12	15,763	6.49429000	0.170 to 0.180	35	0	0.000000000	1.24 to 1.40
13	14,712	6.06128000	0.180 to 0.190	36	1	0.000411996	1.40 to 1.56
14	12,078	4.97608000	0.190 to 0.200	37	0	0.000000000	1.56 to 1.72
15	9,109	3.75287000	0.200 to 0.210	38	1	0.000411996	1.72 to 1.88
16	8,391	3.45706000	0.210 to 0.220	39	0	0.000000000	1.88 to 2.04
17	6,576	2.70928000	0.220 to 0.230	40	1	0.000411996	2.04 to 2.20
18	4,911	2.02331000	0.230 to 0.240	41	0	0.000000000	2.20 to 2.36
19	3,007	1.23887000	0.240 to 0.250	42	0	0.000000000	2.36 to 2.52
20	2,400	0.98879000	0.250 to 0.260	43	0	0.000000000	2.52 to 2.68
21	1,963	0.80874700	0.260 to 0.270	44	0	0.000000000	2.68 to 2.84
22	1,341	0.55248600	0.270 to 0.280	45	0	0.000000000	2.84 to 3.00
23	2,257	0.92874000	0.280 to 0.320				

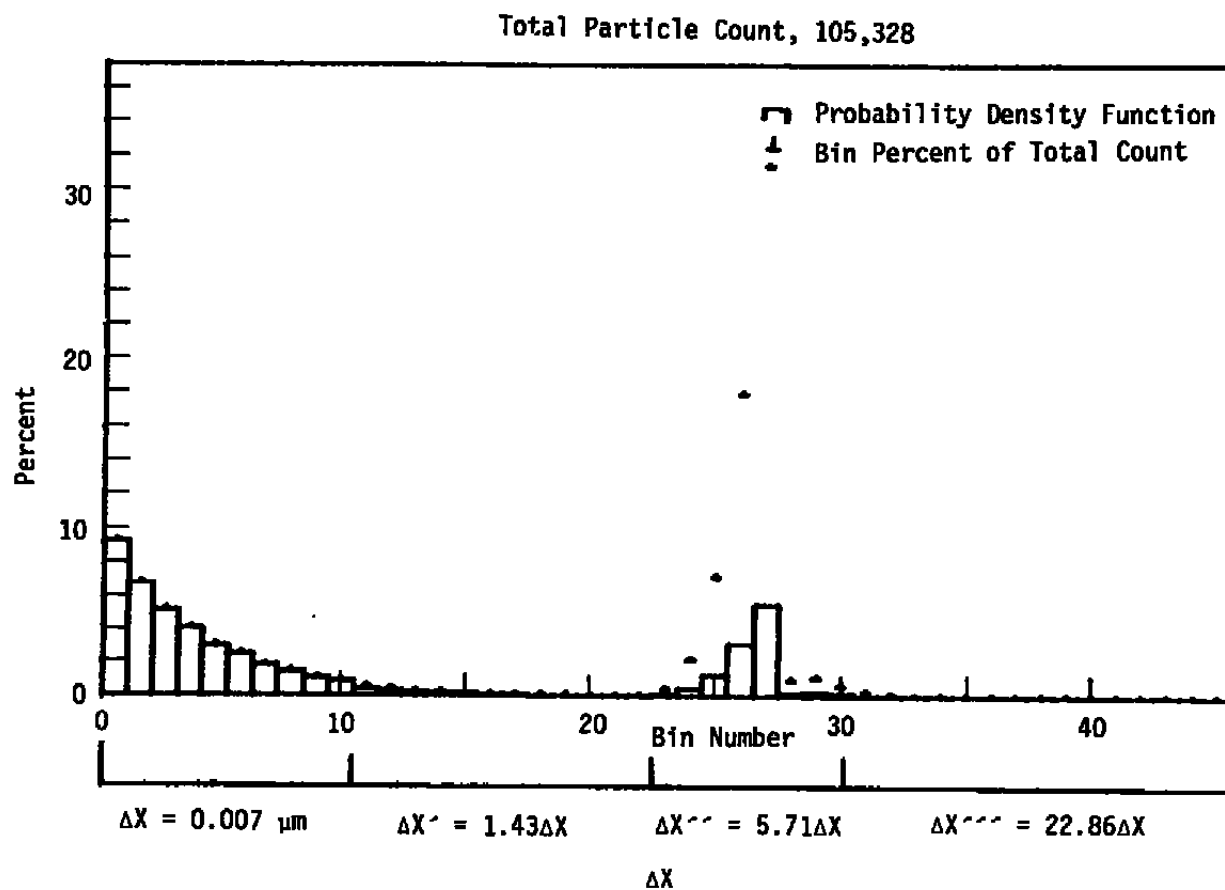
b. 0.176- μ m PSL spheres, concluded
Figure 7. Continued.



c. 0.312- μm PSL spheres
Figure 7. Continued.

<u>Bin</u>	<u>Count</u>	<u>Percent</u>	<u>Size/μm</u>	<u>Bin</u>	<u>Count</u>	<u>Percent</u>	<u>Size/μm</u>
1	2,874	4.06656000	0.090 to 0.097	24	2,551	3.60953000	0.32 to 0.36
2	2,133	3.01808000	0.097 to 0.104	25	1,251	1.77010000	0.36 to 0.40
3	1,586	2.24411000	0.104 to 0.111	26	371	0.52494600	0.40 to 0.44
4	1,155	1.63426000	0.111 to 0.118	27	160	0.22639200	0.44 to 0.48
5	932	1.31873000	0.118 to 0.125	28	67	0.09480150	0.48 to 0.52
6	703	0.99470800	0.125 to 0.132	29	40	0.05659790	0.52 to 0.56
7	554	0.78388100	0.132 to 0.139	30	13	0.01839430	0.56 to 0.60
8	460	0.65087600	0.139 to 0.146	31	30	0.04244840	0.60 to 0.76
9	388	0.54900000	0.146 to 0.153	32	10	0.01414950	0.76 to 0.92
10	257	0.36364200	0.153 to 0.160	33	9	0.01273450	0.92 to 1.08
11	132	0.18677300	0.160 to 0.170	34	2	0.00282990	1.08 to 1.24
12	99	0.14008000	0.170 to 0.180	35	0	0.00000000	1.24 to 1.40
13	68	0.09621640	0.180 to 0.190	36	0	0.00000000	1.40 to 1.56
14	47	0.06650250	0.190 to 0.200	37	2	0.00282990	1.56 to 1.72
15	39	0.05518300	0.200 to 0.210	38	0	0.00000000	1.72 to 1.88
16	69	0.09763140	0.210 to 0.220	39	0	0.00000000	1.88 to 2.04
17	89	0.12593000	0.220 to 0.230	40	0	0.00000000	2.04 to 2.20
18	225	0.31836300	0.230 to 0.240	41	0	0.00000000	2.20 to 2.36
19	712	1.00744000	0.240 to 0.250	42	0	0.00000000	2.36 to 2.52
20	1,389	1.96536000	0.250 to 0.260	43	0	0.00000000	2.52 to 2.68
21	2,467	3.49068000	0.260 to 0.270	44	0	0.00000000	2.68 to 2.84
22	4,357	6.16493000	0.270 to 0.280	45	0	0.00000000	2.84 to 3.00
23	45,433	64.28530000	0.280 to 0.320				

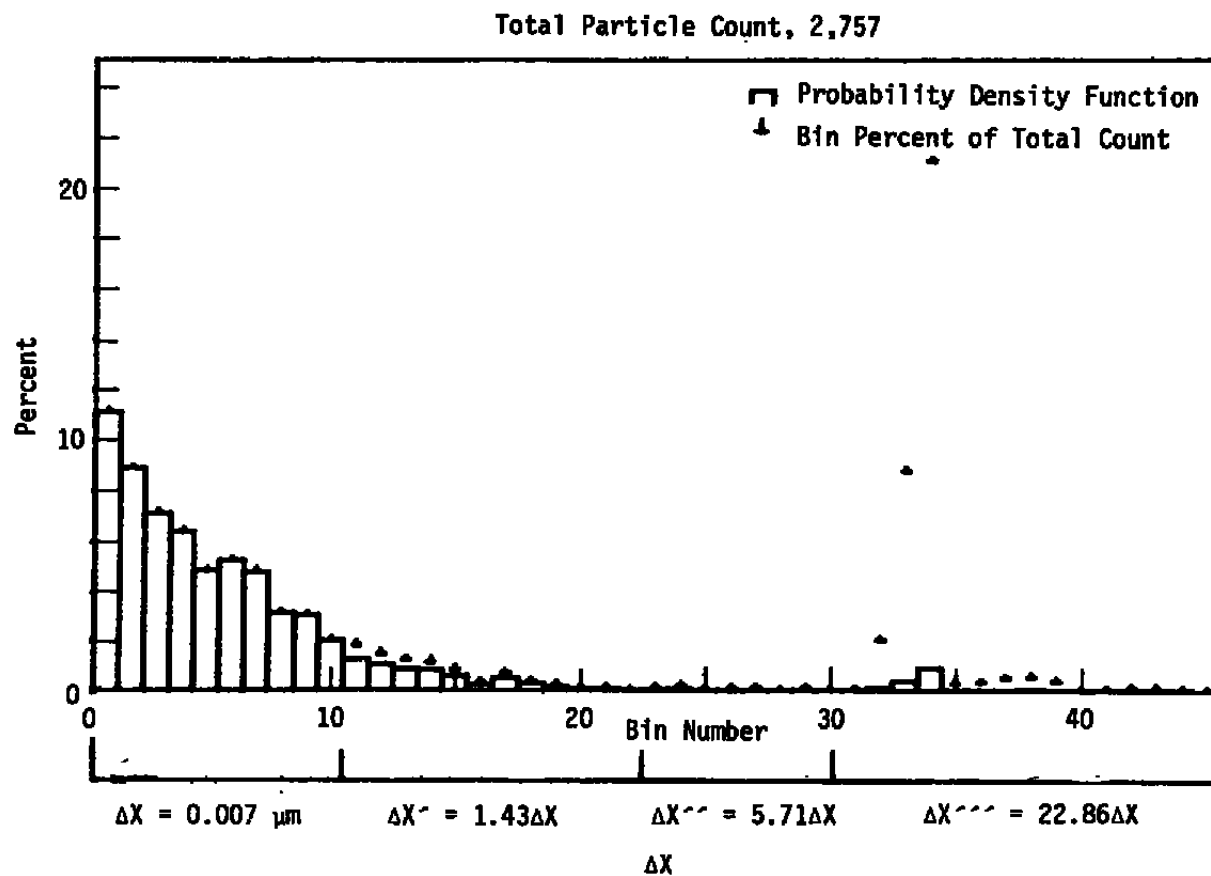
d. 0.312- μ m PSL spheres, concluded
Figure 7. Continued.



e. 0.497- μm PSL spheres
Figure 7. Continued.

<u>Bin</u>	<u>Count</u>	<u>Percent</u>	<u>Size/μm</u>	<u>Bin</u>	<u>Count</u>	<u>Percent</u>	<u>Size/μm</u>
1	9,726	9.234010000	0.090 to 0.097	24	2,286	2.170360000	0.32 to 0.36
2	7,131	6.770280000	0.097 to 0.104	25	7,556	7.173780000	0.36 to 0.40
3	5,483	5.205640000	0.104 to 0.111	26	18,918	17.961000000	0.40 to 0.44
4	4,291	4.073940000	0.111 to 0.118	27	33,122	31.446500000	0.44 to 0.48
5	3,184	3.022940000	0.118 to 0.125	28	1,002	0.951314000	0.48 to 0.52
6	2,627	2.494110000	0.125 to 0.132	29	1,152	1.093730000	0.52 to 0.56
7	1,951	1.852310000	0.132 to 0.139	30	640	0.607626000	0.56 to 0.60
8	1,541	1.463050000	0.139 to 0.146	31	254	0.241151000	0.60 to 0.76
9	1,152	1.093730000	0.146 to 0.153	32	65	0.061712000	0.76 to 0.92
10	910	0.863968000	0.153 to 0.160	33	18	0.017089500	0.92 to 1.08
11	568	0.539268000	0.160 to 0.170	34	7	0.006645910	1.08 to 1.24
12	442	0.419642000	0.170 to 0.180	35	1	0.000949415	1.24 to 1.40
13	274	0.260140000	0.180 to 0.190	36	0	0.000000000	1.40 to 1.56
14	203	0.192731000	0.190 to 0.200	37	3	0.000284825	1.56 to 1.72
15	155	0.147159000	0.200 to 0.210	38	1	0.000949415	1.72 to 1.88
16	79	0.075003800	0.210 to 0.220	39	0	0.000000000	1.88 to 2.04
17	53	0.050319000	0.220 to 0.230	40	0	0.000000000	2.04 to 2.20
18	37	0.035128400	0.230 to 0.240	41	0	0.000000000	2.20 to 2.36
19	32	0.030381300	0.240 to 0.250	42	0	0.000000000	2.36 to 2.52
20	21	0.019937700	0.250 to 0.260	43	0	0.000000000	2.52 to 2.68
21	20	0.018988300	0.260 to 0.270	44	0	0.000000000	2.68 to 2.84
22	20	0.189883000	0.270 to 0.280	45	0	0.000000000	2.84 to 3.00
23	403	0.382614000	0.280 to 0.320				

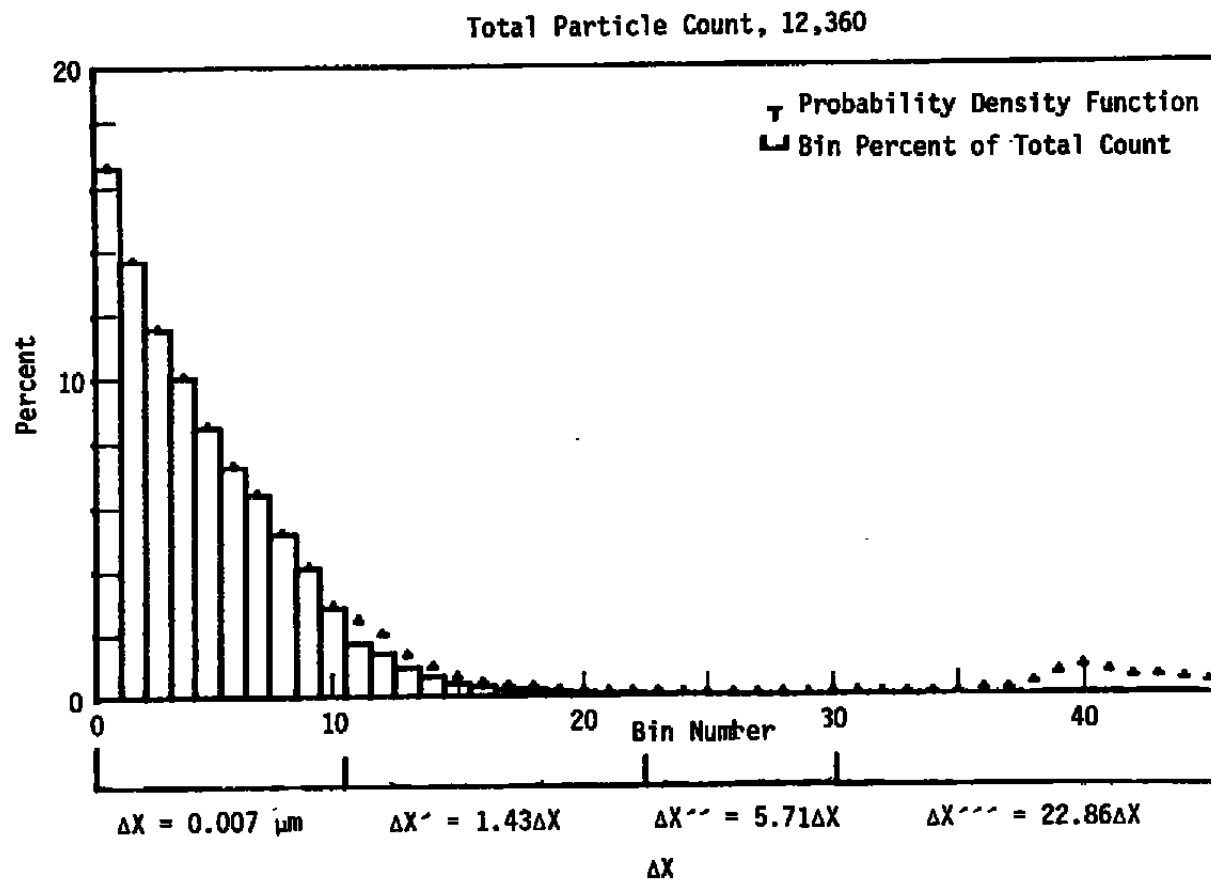
f. 0.497- μ m PSL spheres, concluded
Figure 7. Continued.



g. 1.091- μm PSL spheres
Figure 7. Continued.

<u>Bin</u>	<u>Count</u>	<u>Percent</u>	<u>Size/μm</u>	<u>Bin</u>	<u>Count</u>	<u>Percent</u>	<u>Size/μm</u>
1	308	11.1716000	0.090 to 0.097	24	5	0.1813570	0.32 to 0.36
2	246	8.9227400	0.097 to 0.104	25	1	0.0362713	0.36 to 0.40
3	197	7.1454500	0.104 to 0.111	26	2	0.0725426	0.40 to 0.44
4	177	6.4200200	0.111 to 0.118	27	2	0.0725426	0.44 to 0.48
5	134	4.8603600	0.118 to 0.125	28	0	0.0000000	0.48 to 0.52
6	145	5.2593400	0.125 to 0.132	29	2	0.0725426	0.52 to 0.56
7	133	4.8240800	0.132 to 0.139	30	0	0.0000000	0.56 to 0.60
8	87	3.1556000	0.139 to 0.146	31	1	0.0362713	0.60 to 0.76
9	84	3.0467900	0.146 to 0.153	32	57	2.0674600	0.76 to 0.92
10	56	2.0311900	0.153 to 0.160	33	244	8.8502000	0.92 to 1.08
11	51	1.8498400	0.160 to 0.170	34	583	21.1462000	1.08 to 1.24
12	41	1.4871200	0.170 to 0.180	35	8	0.2901700	1.24 to 1.40
13	34	1.2332200	0.180 to 0.190	36	9	0.3264420	1.40 to 1.56
14	32	1.1606800	0.190 to 0.200	37	14	0.5077980	1.56 to 1.72
15	23	0.8342400	0.200 to 0.210	38	15	0.5440700	1.72 to 1.88
16	9	0.3264420	0.210 to 0.220	39	10	0.3627130	1.88 to 2.04
17	19	0.6891550	0.220 to 0.230	40	0	0.0000000	2.04 to 2.20
18	10	0.3627130	0.230 to 0.240	41	1	0.0362713	2.20 to 2.36
19	6	0.2176280	0.240 to 0.250	42	2	0.0725426	2.36 to 2.52
20	2	0.0725426	0.250 to 0.260	43	2	0.0725426	2.52 to 2.68
21	2	0.0725426	0.260 to 0.270	44	1	0.0362713	2.68 to 2.84
22	0	0.0000000	0.270 to 0.280	45	0	0.0000000	2.84 to 3.00
23	2	0.0725426	0.280 to 0.320				

h. 1.091-μm PSL spheres, concluded
Figure 7. Continued.



i. 2.02- μm PSL spheres
 Figure 7. Continued.

<u>Bin</u>	<u>Count</u>	<u>Percent</u>	<u>Size/μm</u>	<u>Bin</u>	<u>Count</u>	<u>Percent</u>	<u>Size/μm</u>
1	2,054	16.6181000	0.090 to 0.097	24	6	0.0485437	0.32 to 0.36
2	1,694	13.7055000	0.097 to 0.104	25	5	0.0404531	0.36 to 0.40
3	1,431	11.5777000	0.104 to 0.111	26	5	0.0404531	0.40 to 0.44
4	1,245	10.0728000	0.111 to 0.118	27	5	0.0404531	0.44 to 0.48
5	1,051	8.5032400	0.118 to 0.125	28	5	0.0404531	0.48 to 0.52
6	899	7.2734600	0.125 to 0.132	29	2	0.0161812	0.52 to 0.56
7	790	6.3915900	0.132 to 0.139	30	6	0.0485437	0.56 to 0.60
8	640	5.1779900	0.139 to 0.146	31	6	0.0485437	0.60 to 0.76
9	505	4.0857600	0.146 to 0.153	32	2	0.0161812	0.76 to 0.92
10	353	2.8559900	0.153 to 0.160	33	3	0.0242718	0.92 to 1.08
11	300	2.4271800	0.160 to 0.170	34	3	0.0242718	1.08 to 1.24
12	244	1.9741100	0.170 to 0.180	35	5	0.0404531	1.24 to 1.40
13	160	1.2945000	0.180 to 0.190	36	18	0.1456310	1.40 to 1.56
14	110	0.8899680	0.190 to 0.200	37	17	0.1375400	1.56 to 1.72
15	73	0.5906150	0.200 to 0.210	38	44	0.3559870	1.72 to 1.88
16	48	0.3883500	0.210 to 0.220	39	82	0.6634300	1.88 to 2.04
17	34	0.2750810	0.220 to 0.230	40	109	0.8818770	2.04 to 2.20
18	32	0.2589000	0.230 to 0.240	41	86	0.6957930	2.20 to 2.36
19	17	0.1375400	0.240 to 0.250	42	68	0.5501620	2.36 to 2.52
20	13	0.1051780	0.250 to 0.260	43	66	0.5339810	2.52 to 2.68
21	7	0.0566343	0.260 to 0.270	44	56	0.4530740	2.68 to 2.84
22	7	0.0566343	0.270 to 0.280	45	44	0.3559870	2.84 to 3.00
23	10	0.0809061	0.280 to 0.320				

j. 2.02- μ m PS� spheres, concluded

Figure 7. Concluded.

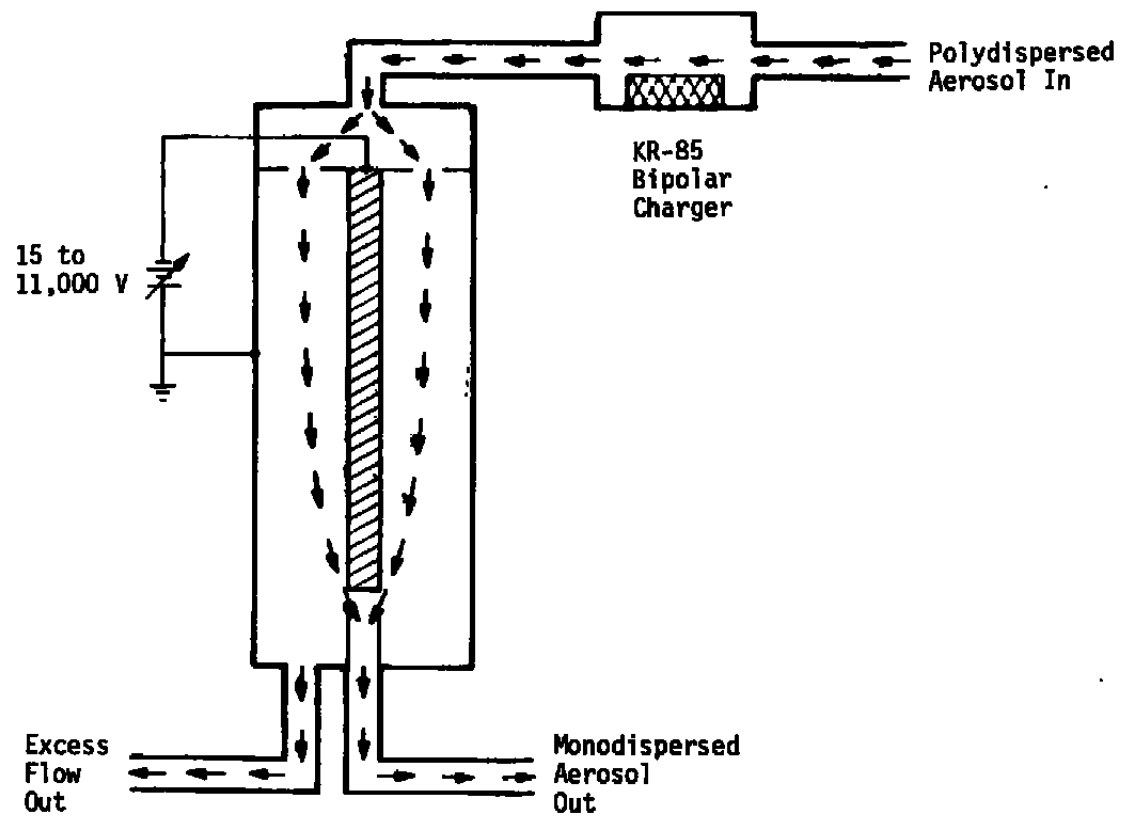
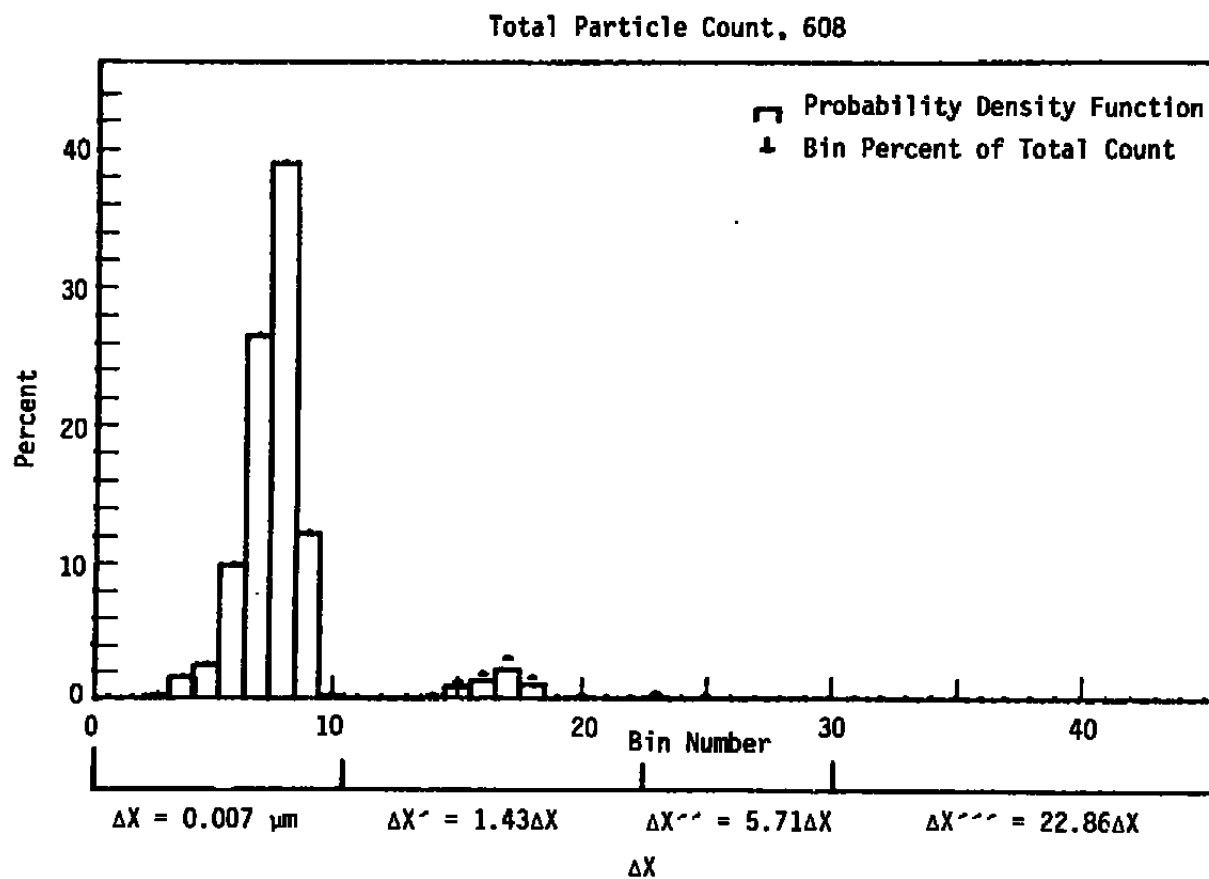


Figure 8. Differential mobility analyzer (DMA).

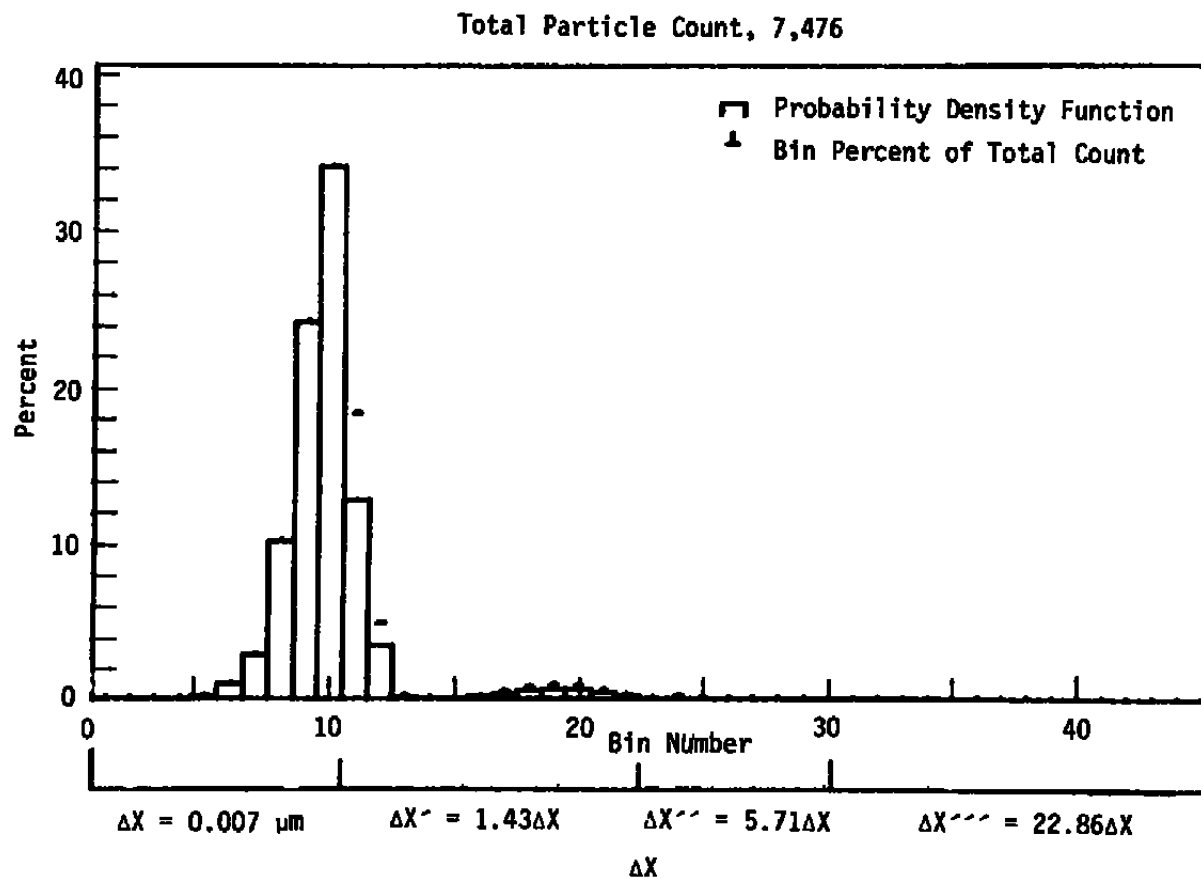


a. Part 1

Figure 9. Nominal 0.18- μm particles produced by the DMA.

<u>Bin</u>	<u>Count</u>	<u>Percent</u>	<u>Size/μm</u>	<u>Bin</u>	<u>Count</u>	<u>Percent</u>	<u>Size/μm</u>
1	0	0.000000	0.090 to 0.097	24	0	0.000000	0.32 to 0.36
2	0	0.000000	0.097 to 0.104	25	1	0.164474	0.36 to 0.40
3	1	0.164474	0.104 to 0.111	26	0	0.000000	0.40 to 0.44
4	9	1.480260	0.111 to 0.118	27	0	0.000000	0.44 to 0.48
5	15	2.467110	0.118 to 0.125	28	0	0.000000	0.48 to 0.52
6	60	9.868420	0.125 to 0.132	29	0	0.000000	0.52 to 0.56
7	161	26.480300	0.132 to 0.139	30	0	0.000000	0.56 to 0.60
8	237	38.980300	0.139 to 0.146	31	0	0.000000	0.60 to 0.76
9	74	12.171100	0.146 to 0.153	32	0	0.000000	0.76 to 0.92
10	1	0.164474	0.153 to 0.160	33	0	0.000000	0.92 to 1.08
11	0	0.000000	0.160 to 0.170	34	0	0.000000	1.08 to 1.24
12	0	0.000000	0.170 to 0.180	35	0	0.000000	1.24 to 1.40
13	0	0.000000	0.180 to 0.190	36	0	0.000000	1.40 to 1.56
14	1	0.164474	0.190 to 0.200	37	0	0.000000	1.56 to 1.72
15	7	1.151320	0.200 to 0.210	38	0	0.000000	1.72 to 1.88
16	11	1.809210	0.210 to 0.220	39	0	0.000000	1.88 to 2.04
17	18	2.960530	0.220 to 0.230	40	0	0.000000	2.04 to 2.20
18	9	1.480260	0.230 to 0.240	41	0	0.000000	2.20 to 2.36
19	0	0.000000	0.240 to 0.250	42	0	0.000000	2.36 to 2.52
20	1	0.164474	0.250 to 0.260	43	0	0.000000	2.52 to 2.68
21	0	0.000000	0.260 to 0.270	44	0	0.000000	2.68 to 2.84
22	0	0.000000	0.270 to 0.280	45	0	0.000000	2.84 to 3.00
23	2	0.328947	0.280 to 0.320				

b. Part 2
Figure 9. Concluded.



a. Part 1

Figure 10. Nominal 0.199- μm particles produced by the DMA.

<u>Bin</u>	<u>Count</u>	<u>Percent</u>	<u>Size/μm</u>	<u>Bin</u>	<u>Count</u>	<u>Percent</u>	<u>Size/μm</u>
1	0	0.0000000	0.090 to 0.097	24	9	0.1203850	0.320 to 0.360
2	0	0.0000000	0.097 to 0.104	25	5	0.0668807	0.360 to 0.400
3	1	0.0133761	0.104 to 0.111	26	0	0.0000000	0.400 to 0.440
4	0	0.0000000	0.111 to 0.118	27	0	0.0000000	0.440 to 0.480
5	11	0.1471380	0.118 to 0.125	28	0	0.0000000	0.480 to 0.520
6	69	0.9229530	0.125 to 0.132	29	0	0.0000000	0.520 to 0.560
7	213	2.8491200	0.132 to 0.139	30	0	0.0000000	0.560 to 0.600
8	768	10.2729000	0.139 to 0.146	31	0	0.0000000	0.600 to 0.760
9	1,811	24.2242000	0.146 to 0.153	32	0	0.0000000	0.760 to 0.920
10	2,550	34.1092000	0.153 to 0.160	33	0	0.0000000	0.920 to 1.080
11	1,373	18.3654000	0.160 to 0.170	34	0	0.0000000	1.080 to 1.240
12	370	4.9491700	0.170 to 0.180	35	0	0.0000000	1.240 to 1.400
13	11	0.1471380	0.180 to 0.190	36	0	0.0000000	1.400 to 1.560
14	2	0.2675230	0.190 to 0.200	37	0	0.0000000	0.156 to 1.720
15	2	0.2675230	0.200 to 0.210	38	0	0.0000000	0.172 to 1.880
16	12	0.1605140	0.210 to 0.220	39	0	0.0000000	1.880 to 2.040
17	31	0.4146600	0.220 to 0.230	40	0	0.0000000	2.040 to 2.200
18	53	0.7089350	0.230 to 0.240	41	0	0.0000000	2.200 to 2.360
19	66	0.8828250	0.240 to 0.250	42	0	0.0000000	2.360 to 2.520
20	63	0.8426970	0.250 to 0.260	43	0	0.0000000	2.520 to 2.680
21	36	0.4815410	0.260 to 0.270	44	0	0.0000000	2.680 to 2.840
22	18	0.2407700	0.270 to 0.280	45	0	0.0000000	2.840 to 3.000
23	2	0.0267523	0.280 to 0.320				

b. Part 2
Figure 10. Concluded.

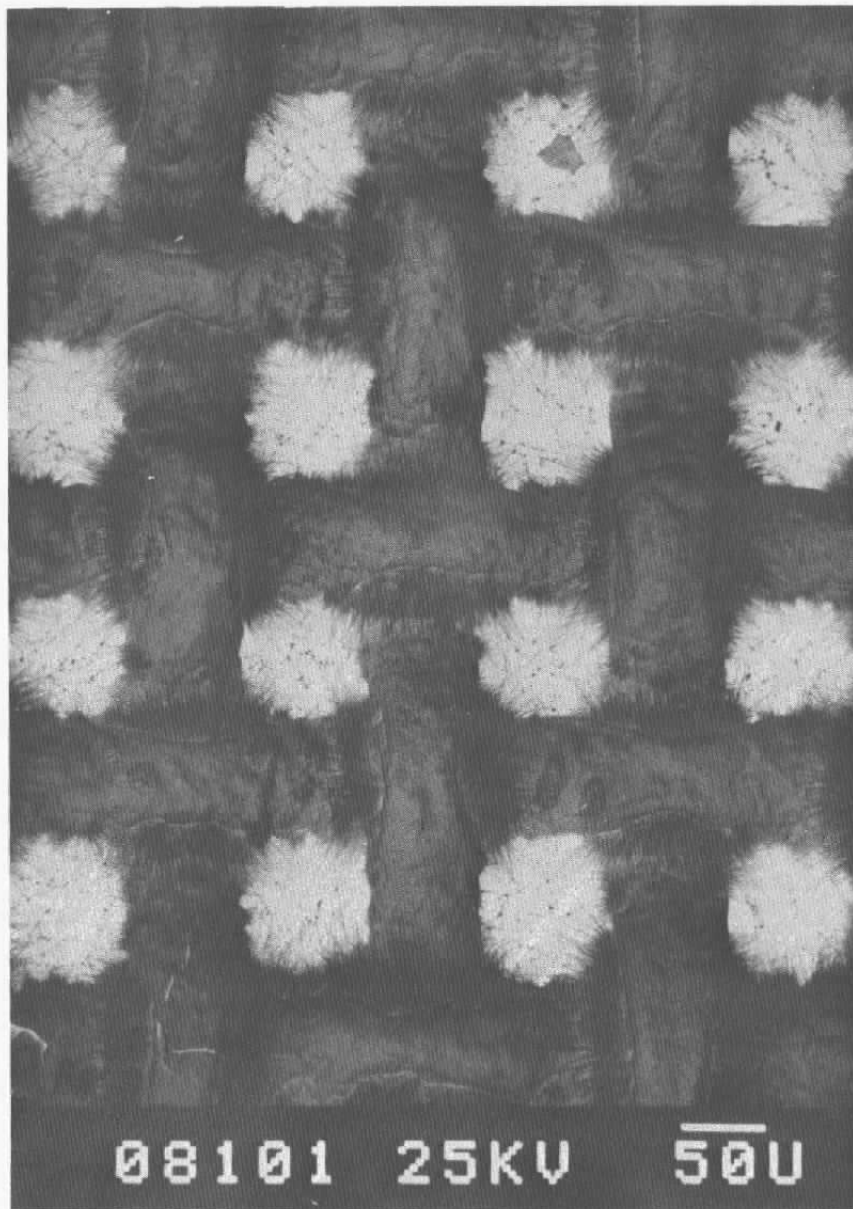


Figure 11. Electron micrograph of a whisker particle collector after particle sampling.

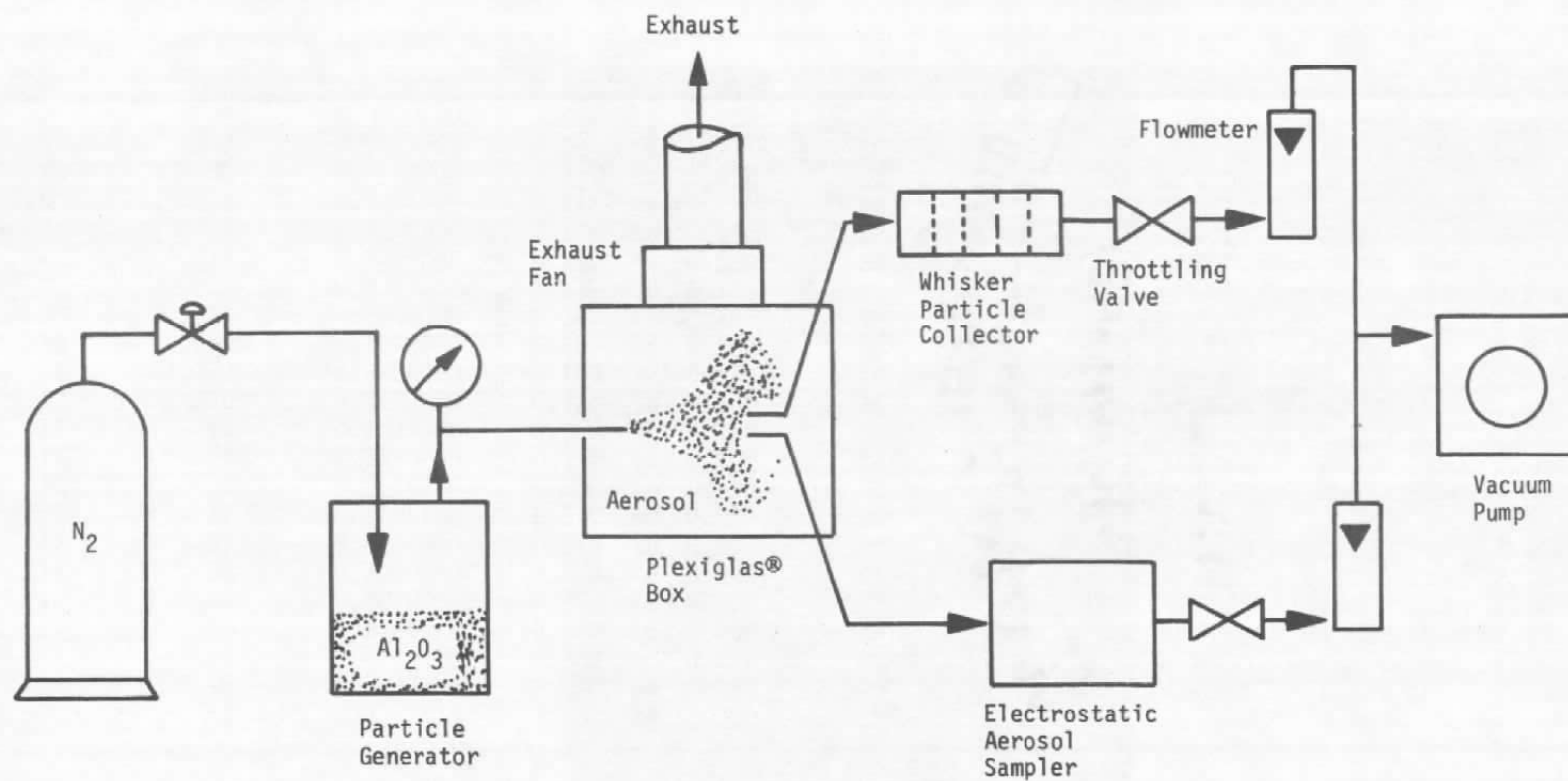


Figure 12. Schematic diagram of the setup for aerosol sampling.

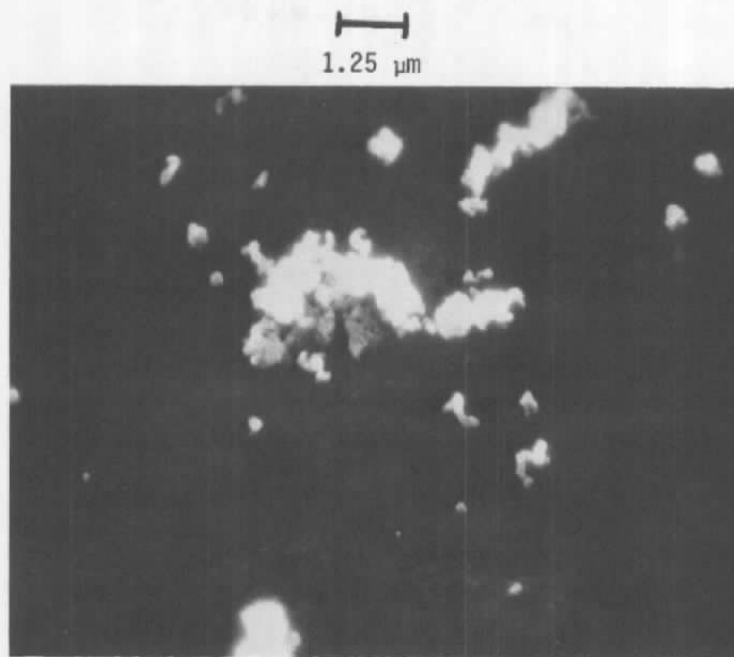


Figure 13. Electron micrograph of Type C 1.0- μ m alumina particles captured by the EAS (magnification, 4,000x).

10 μm



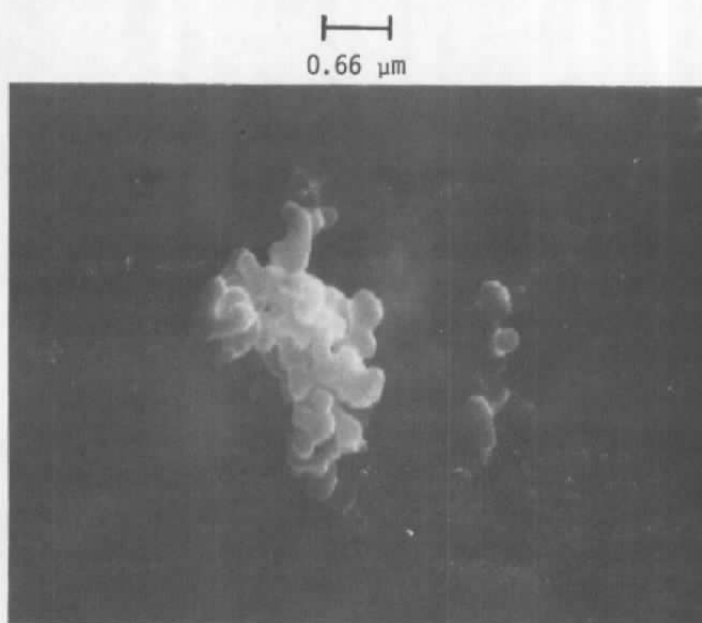
a. Magnification, 1,000x

2.0 μm

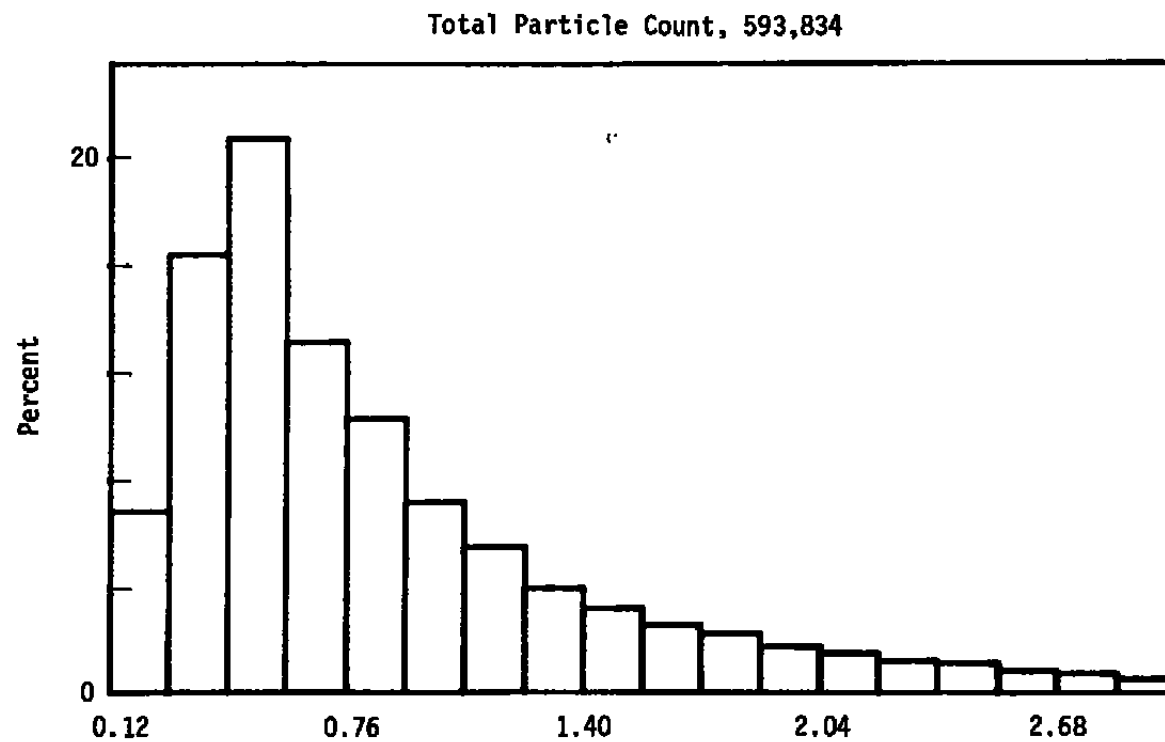


b. Magnification, 5,000x

Figure 14. Electron micrographs of Type A 0.3- μm alumina particles captured by the EAS.

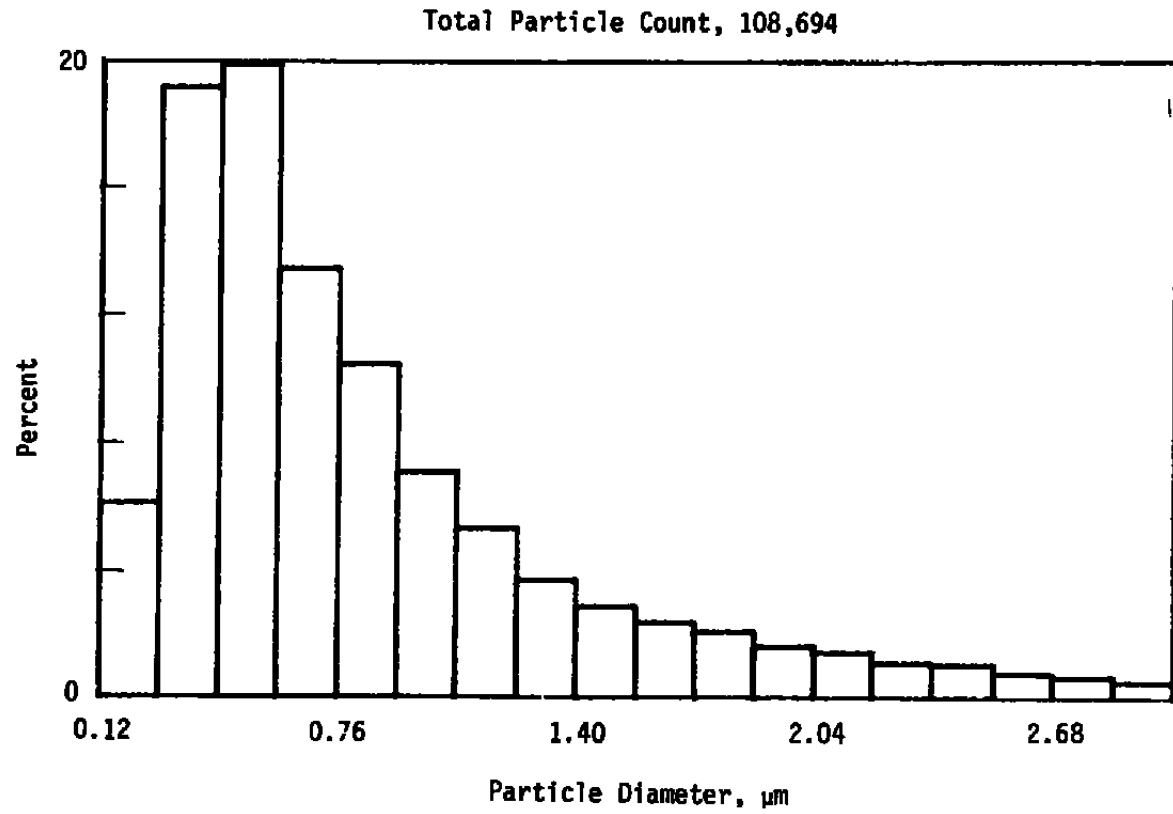


c. Magnification, 15,000x
Figure 14. Concluded.

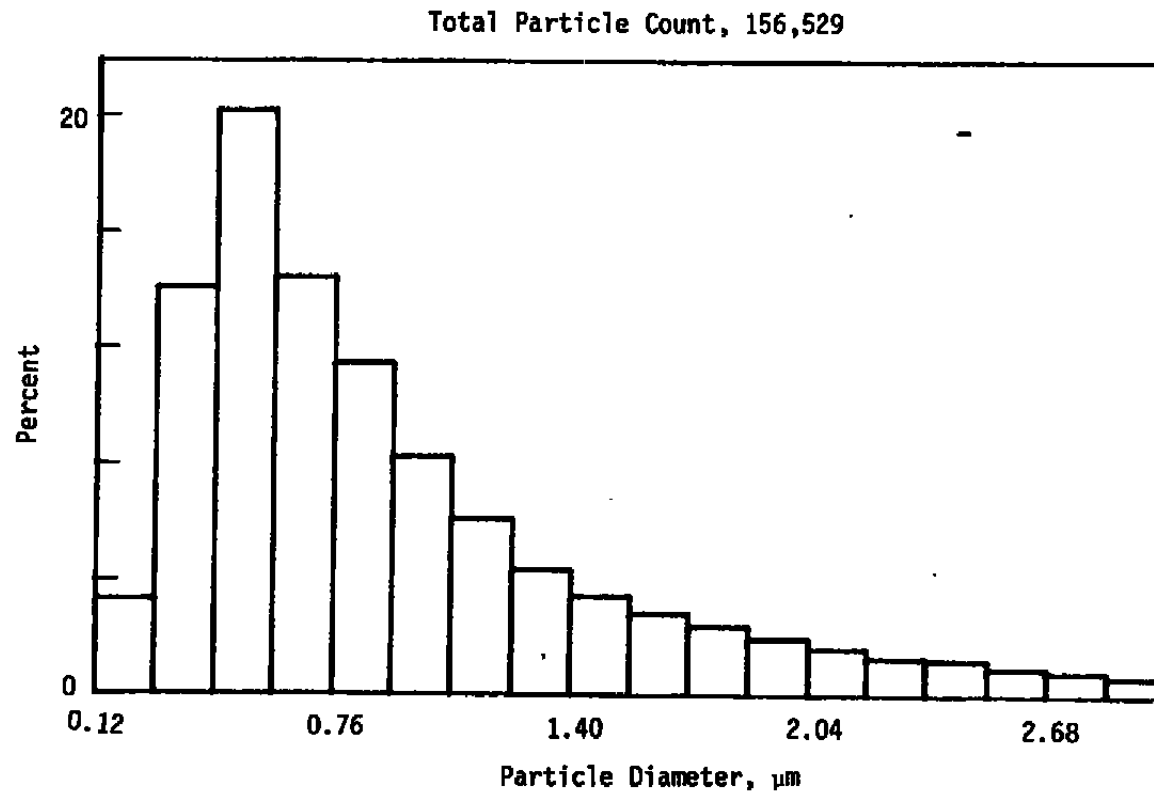


a. Type C 1.0- μm polishing powder

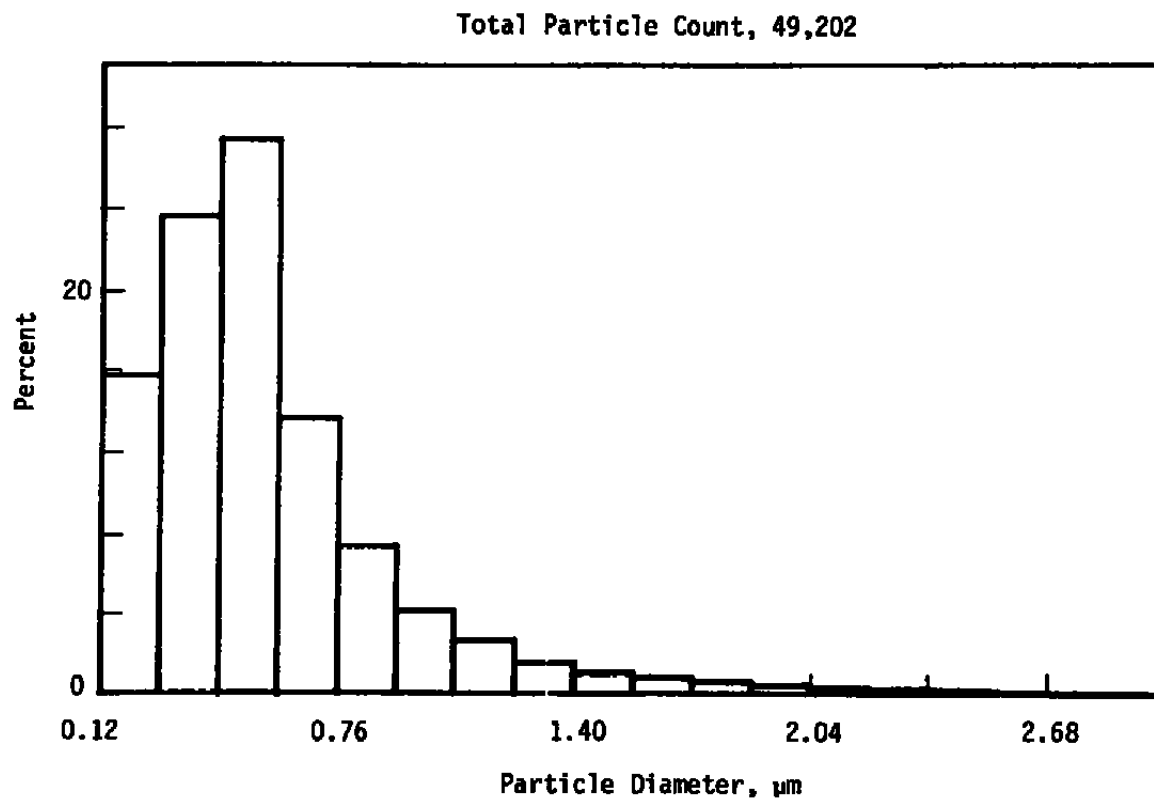
Figure 15. Particle size distributions for various alumina powder aerosols.



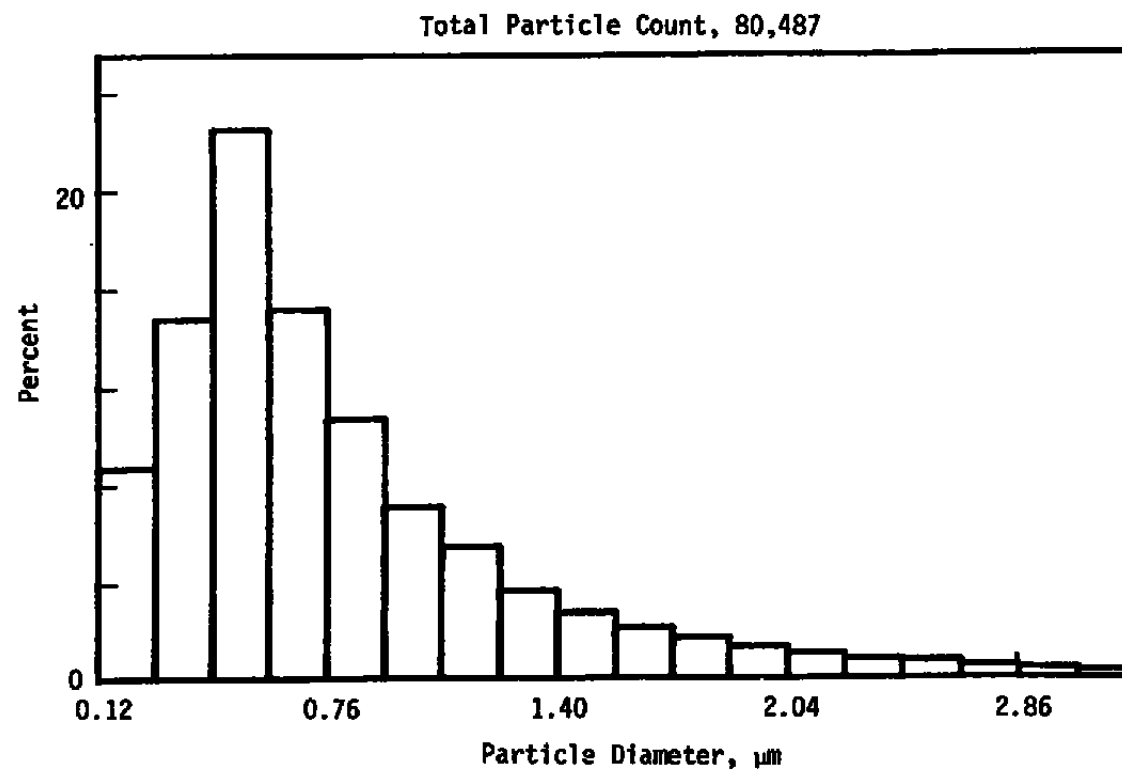
b. Type C 1.0-μm polishing powder with silica flow agent
Figure 15. Continued.



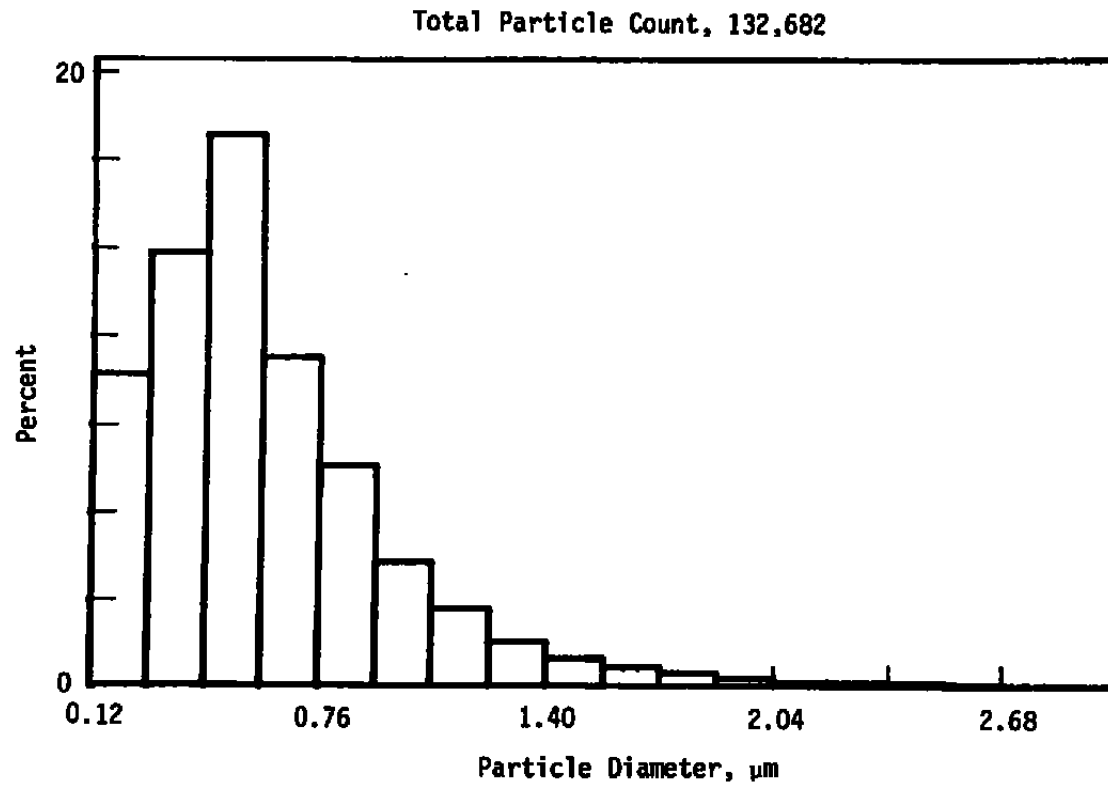
c. Proprietary mixture of 0.7- μm polishing powder and silica flow agent
Figure 15. Continued.



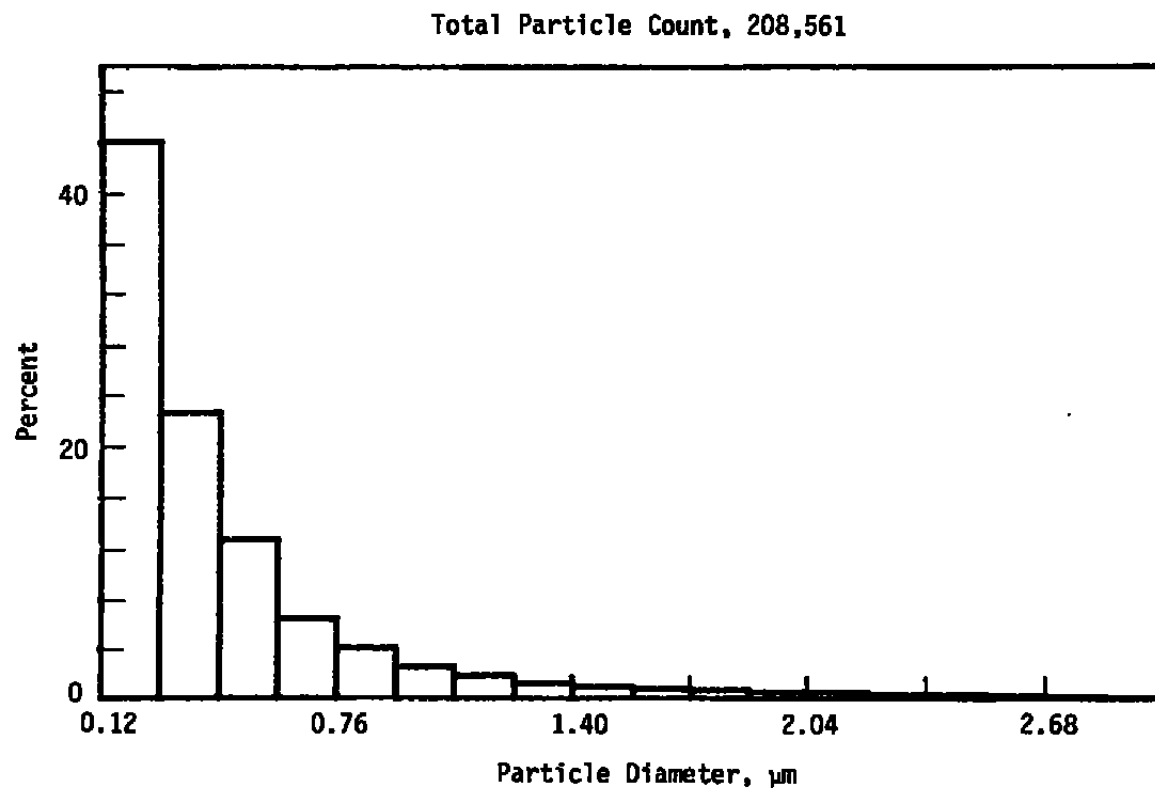
d. Type C 1.0- μm polishing powder aerosol through a sonic orifice
Figure 15. Continued.



e. Type AF 1.0- μm polishing powder
Figure 15. Continued.



f. Type AF 1.0- μm polishing powder aerosol through a sonic orifice
Figure 15. Concluded.

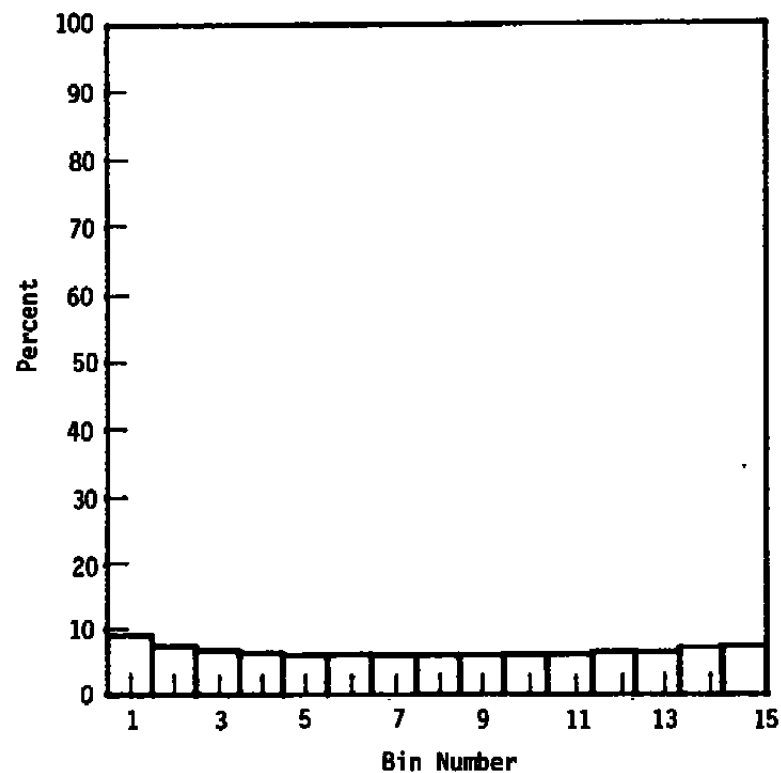


a. Type A polishing powder

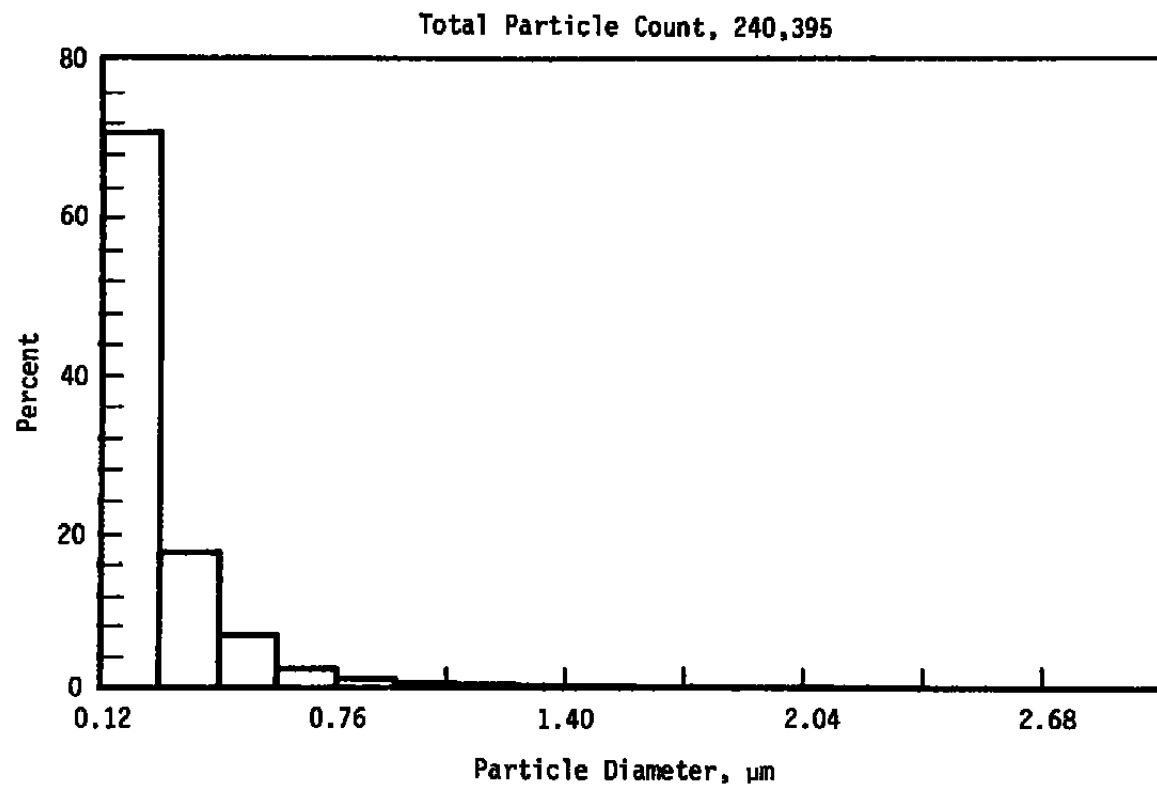
Figure 16. Particle size distributions for various alumina powder aerosols with a nominal size specification of 0.3 μm .

Total Particle Count, 63,159

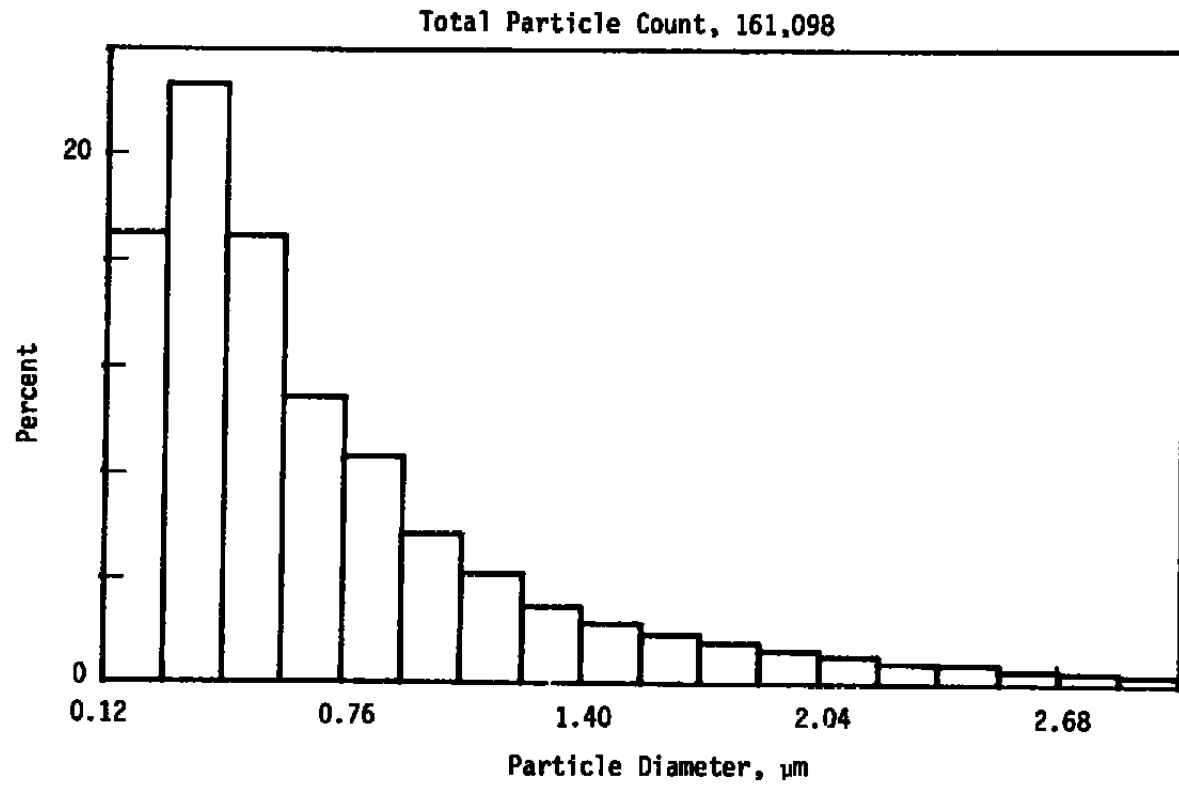
<u>Bin</u>	<u>Count</u>	<u>Percent</u>	<u>Size/μm</u>
1	5,723	9.06126	0.090 to 0.097
2	4,744	7.51120	0.097 to 0.104
3	4,237	6.70847	0.104 to 0.111
4	4,047	6.40764	0.111 to 0.118
5	3,810	6.03239	0.118 to 0.125
6	3,882	6.14639	0.125 to 0.132
7	3,767	5.96431	0.132 to 0.139
8	3,766	5.96273	0.139 to 0.146
9	3,796	6.01023	0.146 to 0.153
10	3,943	6.24297	0.153 to 0.160
11	3,876	6.13689	0.160 to 0.167
12	4,084	6.46622	0.167 to 0.174
13	4,129	6.53747	0.174 to 0.181
14	4,619	7.31329	0.181 to 0.188
15	4,736	7.49854	0.188 to 0.195



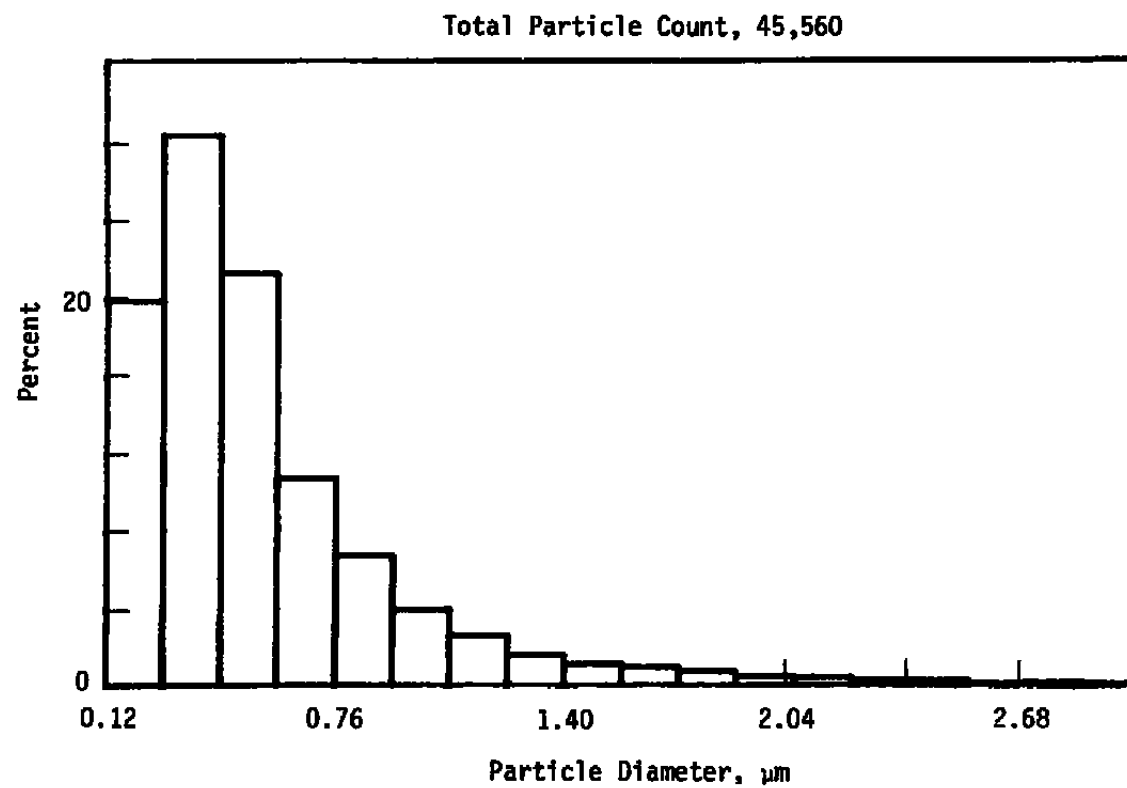
b. Type A polishing powder, high-resolution histogram
Figure 16. Continued.



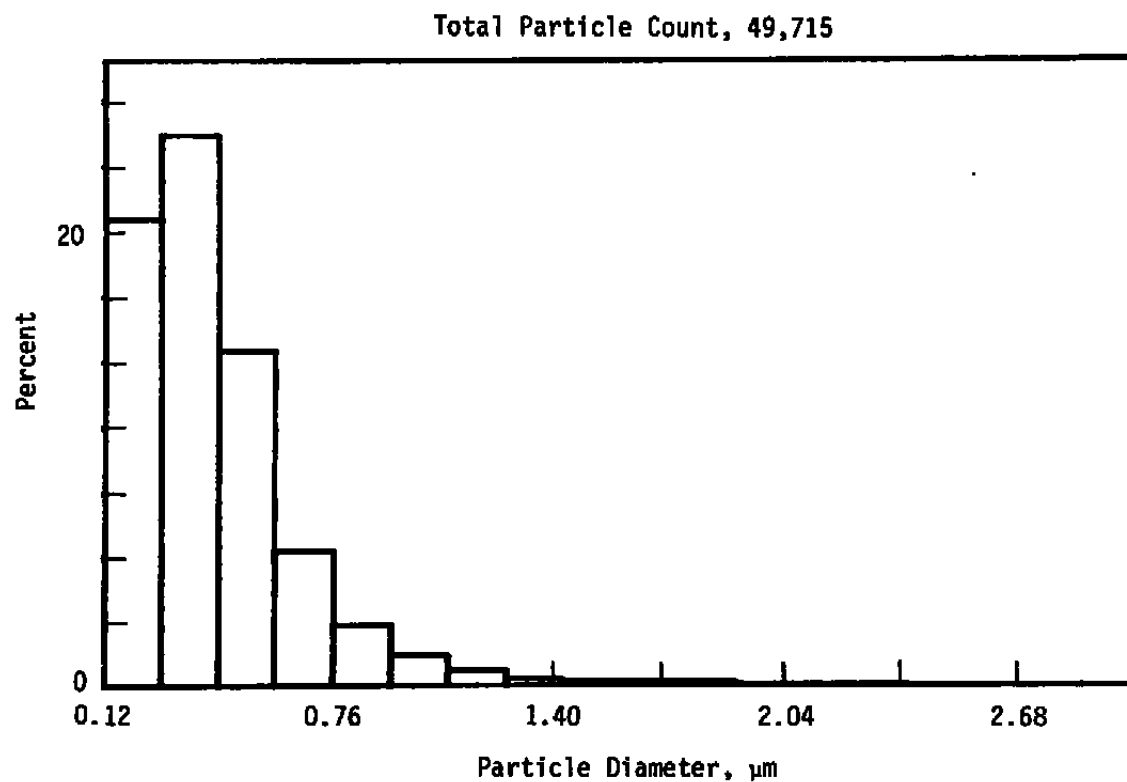
c. Type A polishing powder aerosol through a sonic orifice
Figure 16. Continued.



d. Type SF polishing powder
Figure 16. Continued.



e. Type AF polishing powder
Figure 16. Continued.



f. Type AF polishing powder aerosol through a sonic orifice
Figure 16. Concluded.

Magnification, 20,000x

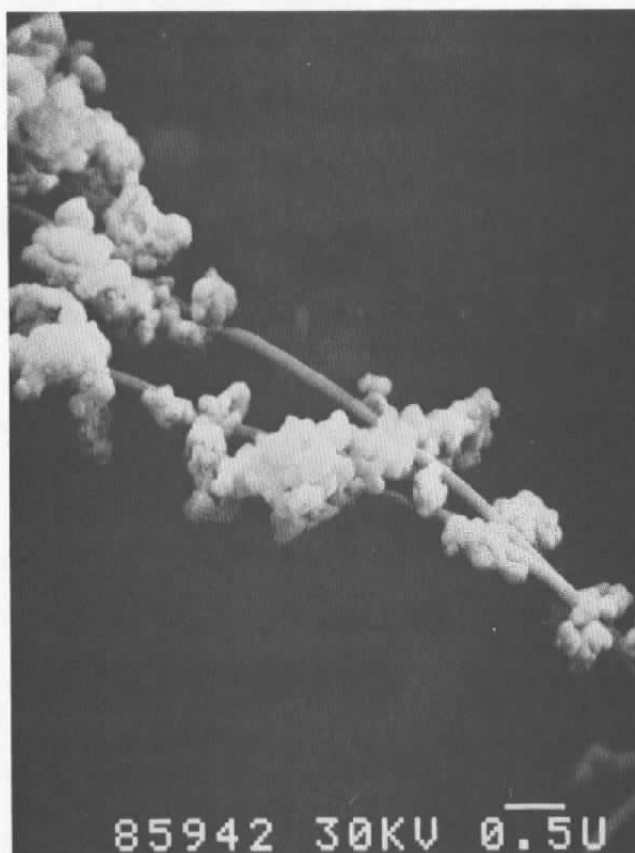


Figure 17. Electron micrograph of the Type A 0.3- μ m alumina particles collected by the WPC.

Magnification, 20,000x

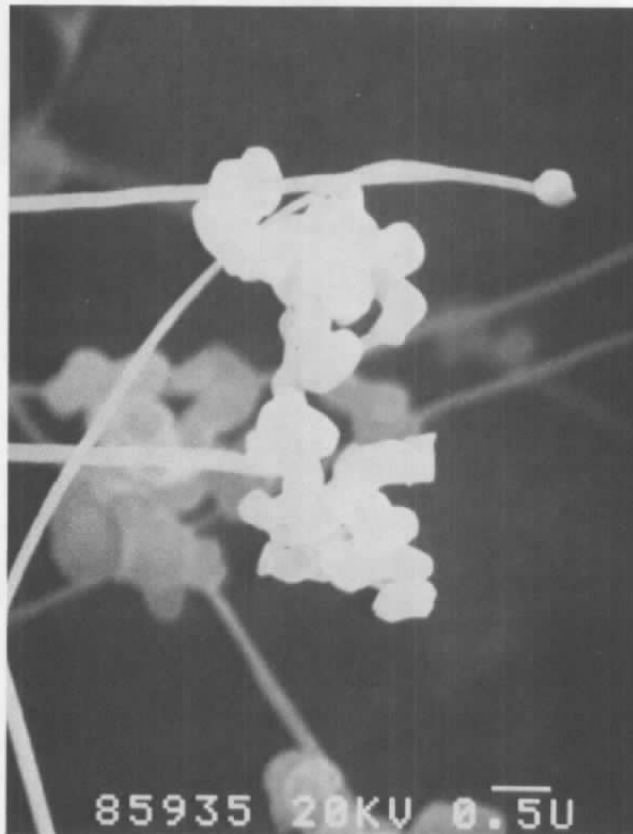


Figure 18. Electron micrograph of the Type C 1.0- μ m alumina particles collected by the WPC.

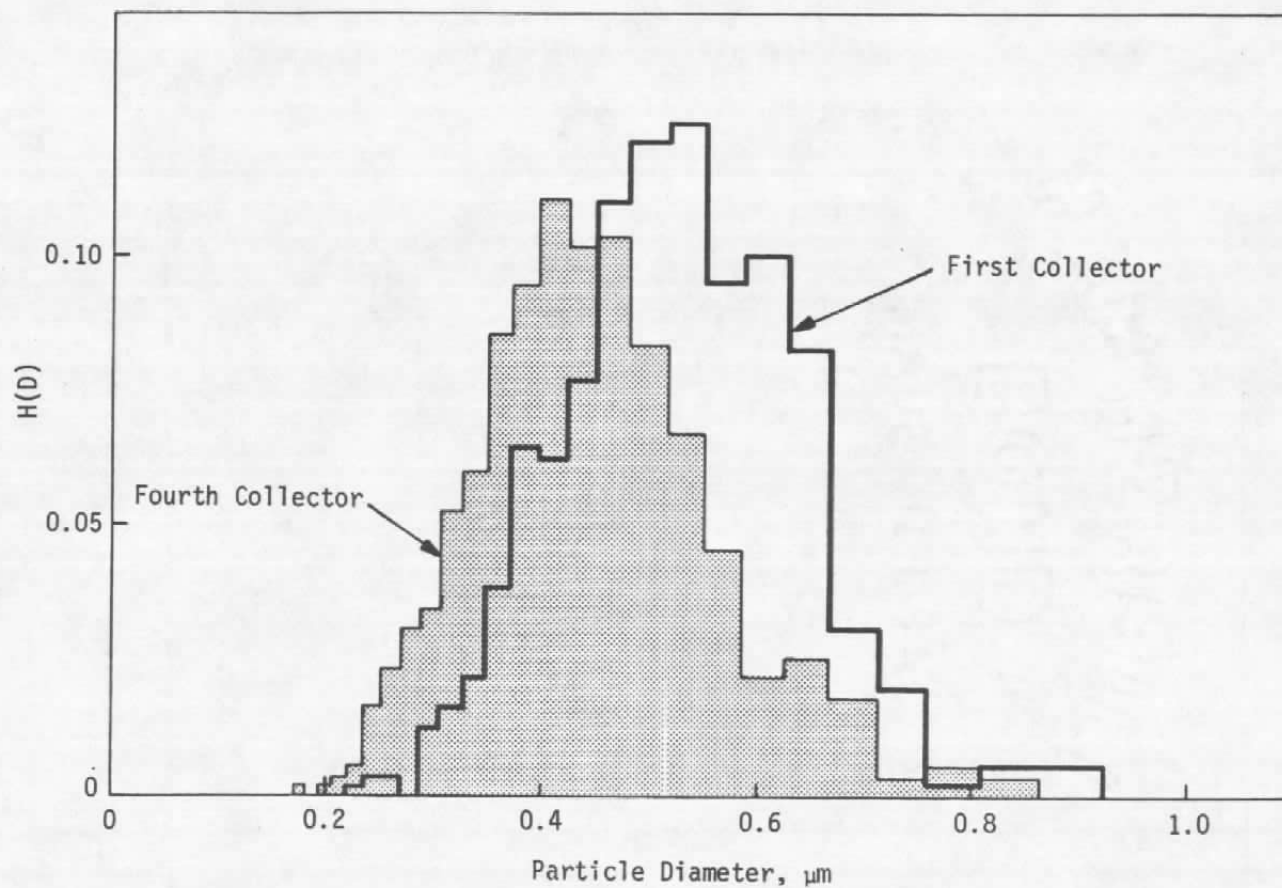


Figure 19. Particle size distribution on the first and fourth collector after sampling the Type C 1.0-μm alumina powder aerosol.

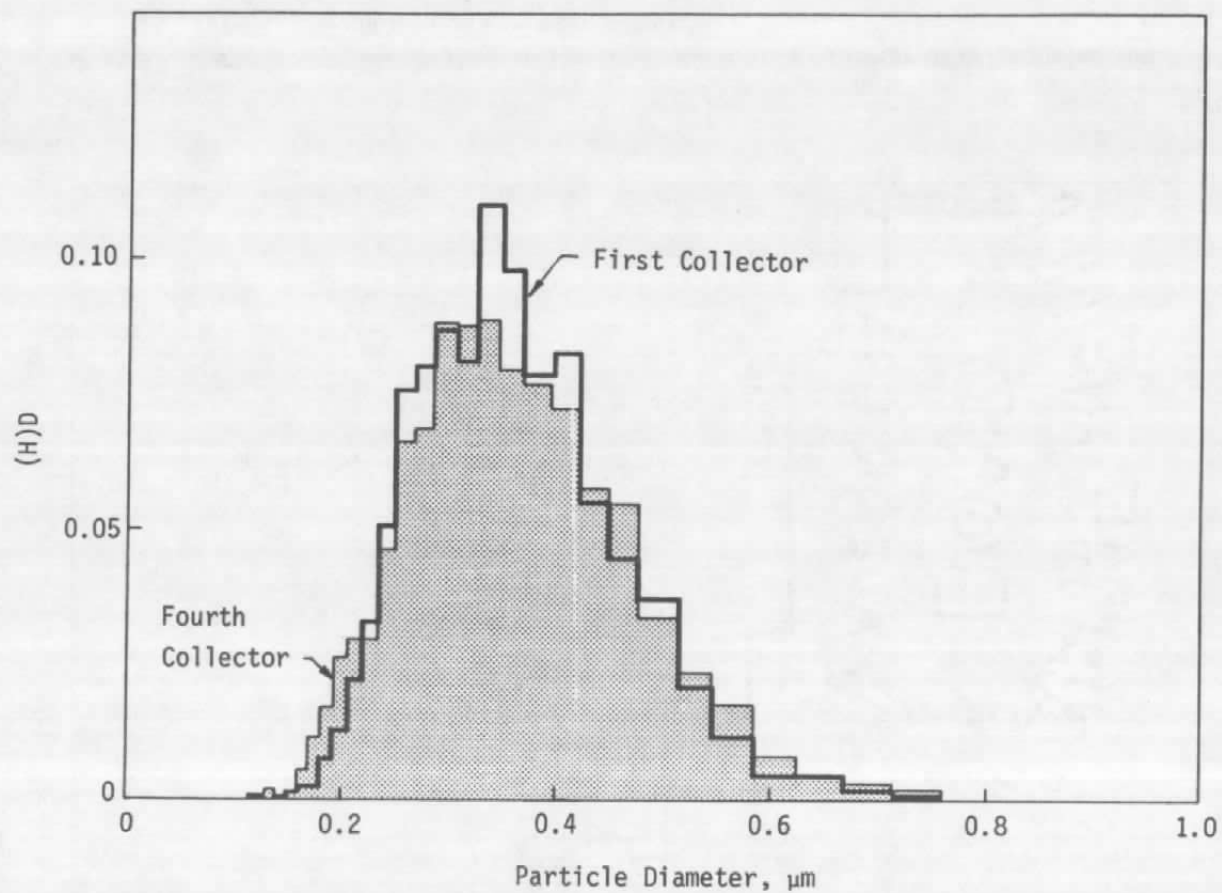


Figure 20. Particle size distribution on the first and fourth collector after sampling the Type A 0.3-μm alumina powder aerosol.

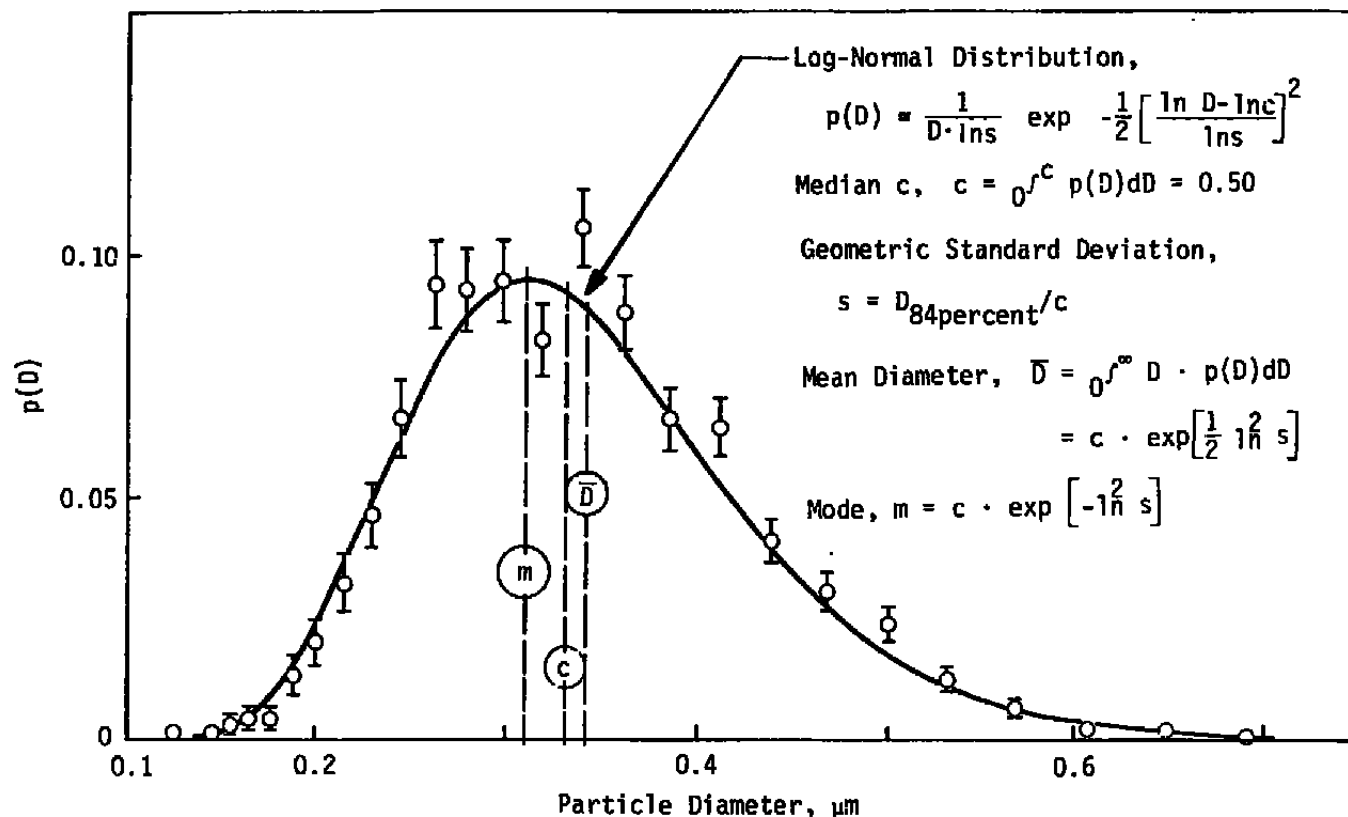


Figure 21. Log-normal distribution function fitted to the WPC particle size distribution for the Type A 0.3- μm alumina powder aerosol.

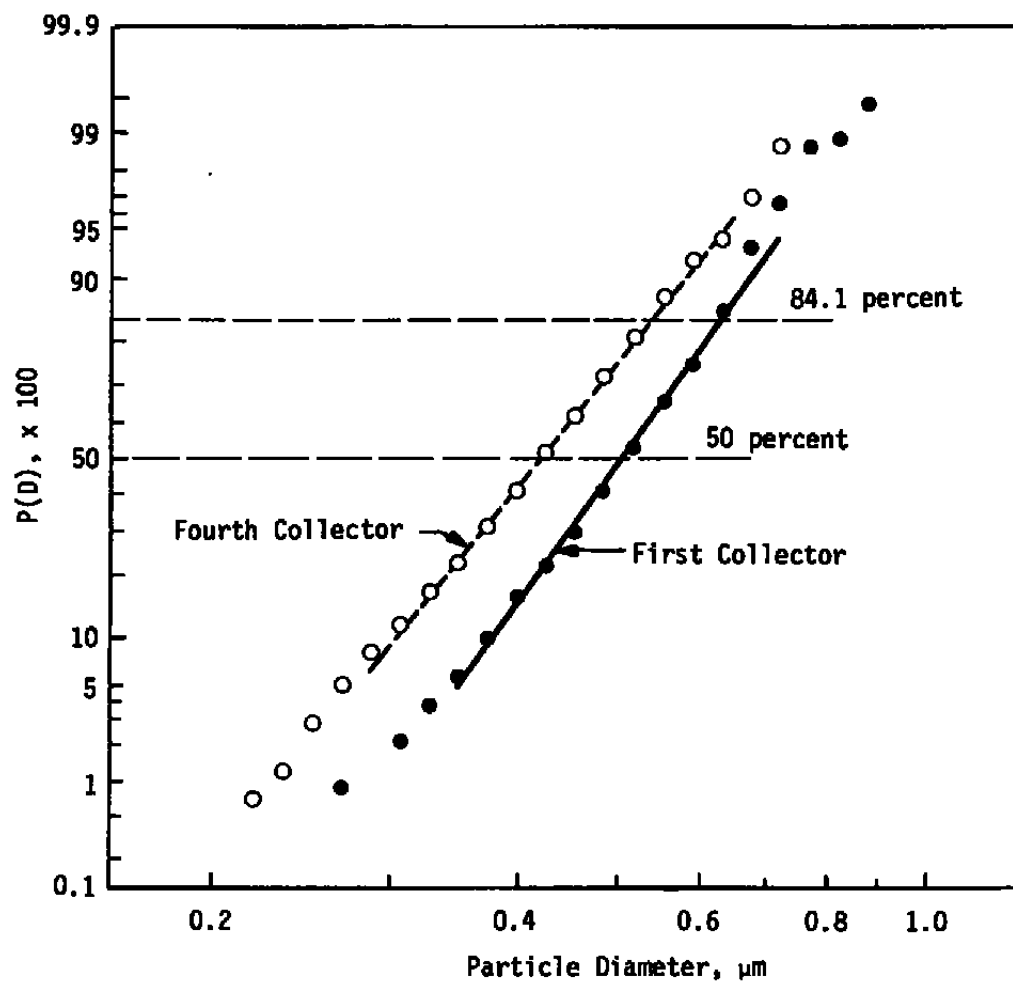


Figure 22. Cumulative percentage distribution plotted on log-probability paper for the Type C 1.0- μm alumina powder aerosol.

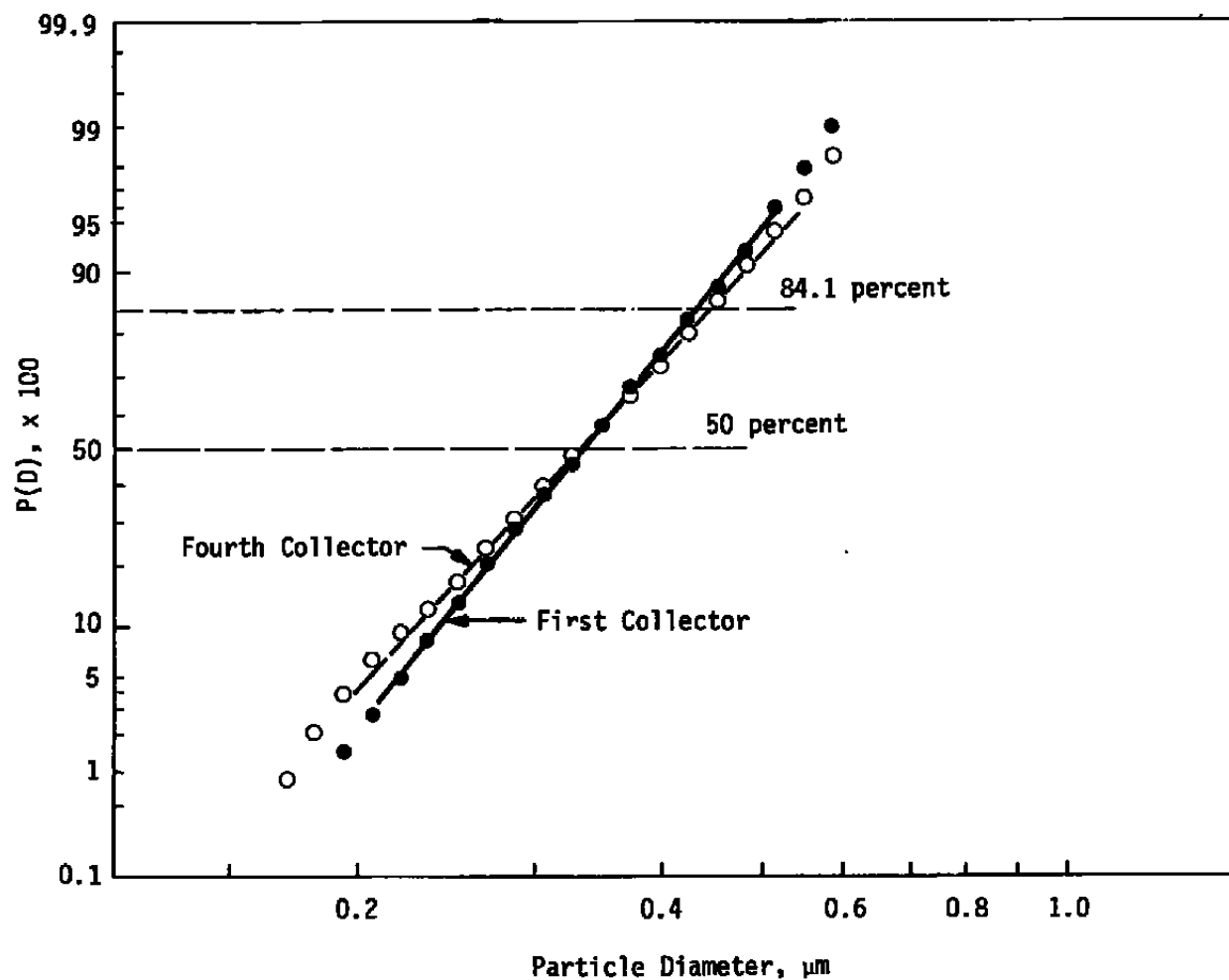


Figure 23. Cumulative percentage distribution plotted on log-probability paper for the Type A 0.3- μm alumina powder aerosol.

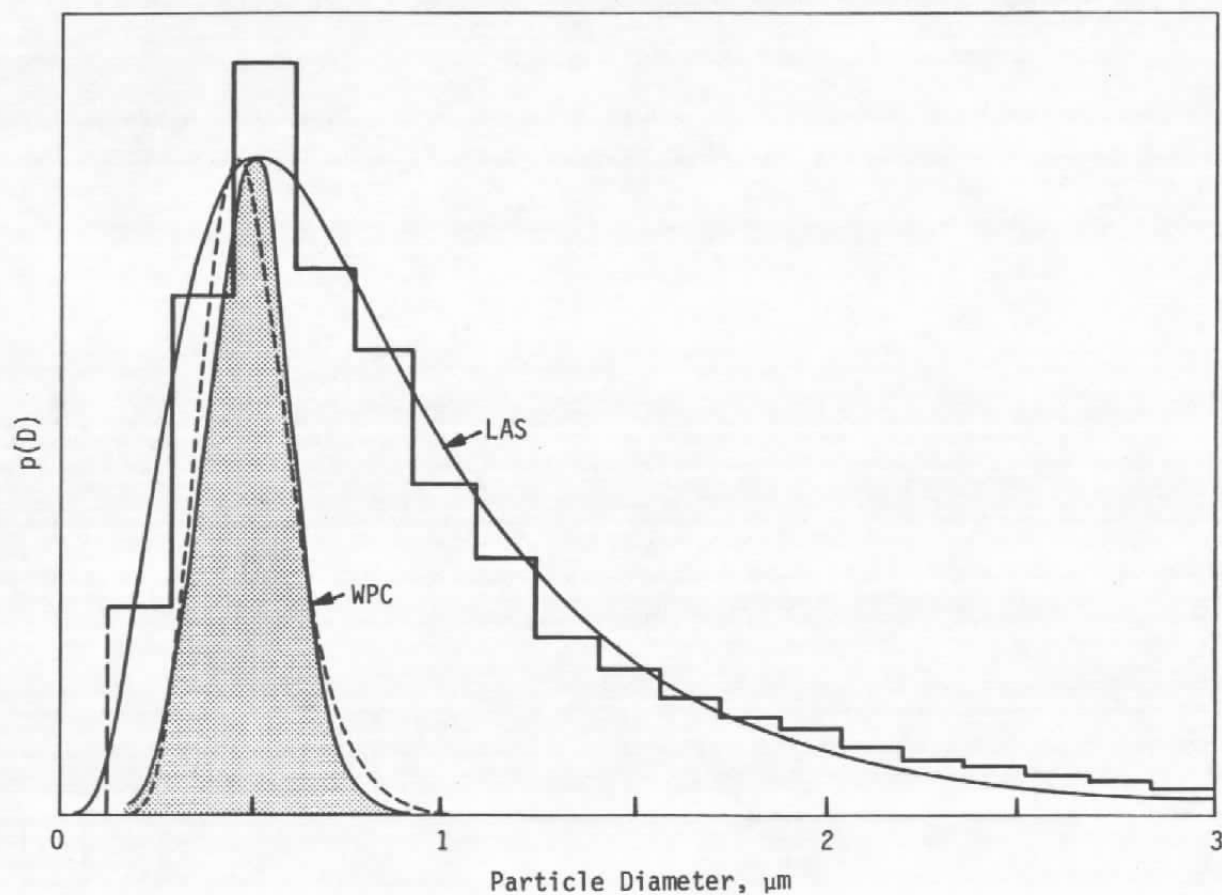


Figure 24. Log-normal functions fitted to the LAS and WPC histograms for the Type C 1.0- μm alumina powder aerosol.

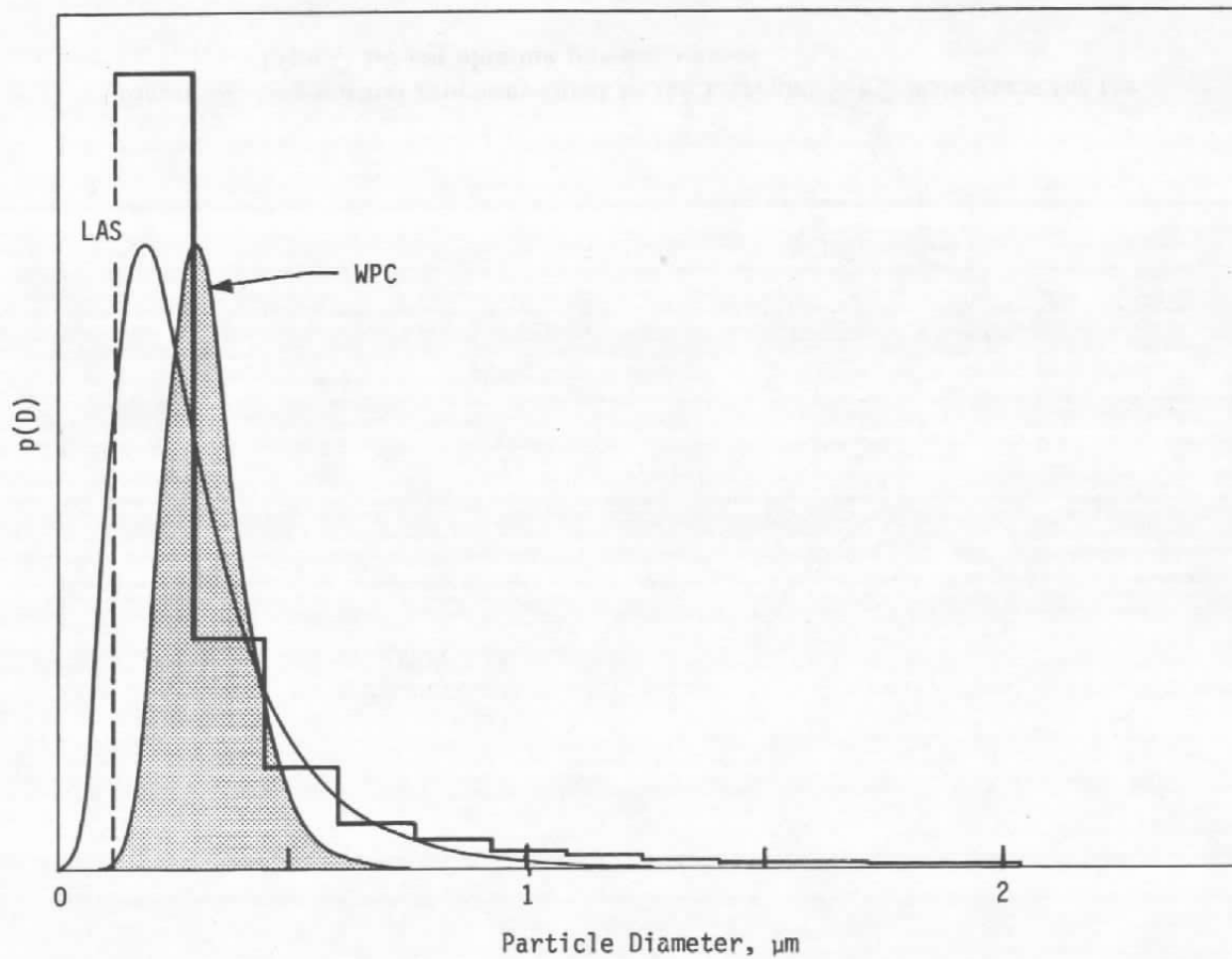


Figure 25. Log-normal functions fitted to the LAS and WPC histograms for the Type A 0.3- μm alumina powder aerosol.

Table 1. Size Distribution Parameters Derived from Laser Aerosol Spectrometer (LAS) and Whisker Particle Collector (WPC) Methods

Material	Method	Mode, $m/\mu\text{m}$	Median $c/\mu\text{m}$	Mean Diameter, $\bar{D}/\mu\text{m}$	Geametry Standard Deviation, s
0.3- μm Al_2O_3	LAS	0.18	0.25	0.30	1.80
	WPC	0.29	0.31	0.32	1.30
1- μm Al_2O_3	LAS	0.50	0.75	0.93	1.90
	WPC	0.45	0.48	0.49	1.28

NOMENCLATURE

DMA	Differential mobility analyzer
EAS	Electrostatic aerosol sampler
KR-85	Radioactive isotope of Krypton gas
LAS	Laser aerosol spectrometer
PSL	Polystyrene latex
SEM	Scanning electron microscope
WPC	Whisker particle capture system
c	Median particle size
\overline{D}	Mean particle diameter
D	Particle diameter
H(D)	Histogram function
m	Mode value
P(D)	Cumulative percentage distribution function
p(D)	Probability density function
s	Geometric standard deviation
α	Coefficient of absorption
η	Efficiency of whisker collector